Chapter 4
Geocell-Reinforced Foundations

Gholamhosein Tavakoli Mehrjardi and Seyed Naser Moghaddas Tafreshi

Keywords Geocell-reinforced foundations · Bearing capacity · Failure mechanism · Scale effect

4.1 Introduction

Constructing over soft soils is a challenge for geotechnical engineers because of the low shear strength of the foundation, which causes excessive consolidation settlements and, sometimes, bearing capacity failure. A variety of ground improvement techniques, including vertical drains, grouting, complete soil replacement, geosynthetic reinforcement, and piling, have been developed to solve the problems (e.g. Liu et al. 2008; Rowe and Taechakumthorn 2008). Among these techniques, geosynthetic reinforcement has been increasingly used as basal reinforcement since it facilitates rapid construction at low costs (Rowe and Li 2005) although care is required when dealing with rate-sensitive soft soils (Li and Rowe 2008). Geocells account geosynthetic products with a three-dimensional cellular network constructed from thin polymeric strips. Many investigators have reported the beneficial use of geocell layer at the base of the embankment. To sum up: as an immediate working platform for the construction, more uniform settlements, reduced construction time and eliminated excavation and replacement costs, increased bearing capacity, and decreased settlements.

G. Tavakoli Mehrjardi
Department of Civil Engineering, Faculty of Engineering, Kharazmi University, Tehran, Iran
e-mail: ghtavakoli@khu.ac.ir

S. N. Moghaddas Tafreshi (✉)
Faculty of Civil Engineering, K.N. Toosi University of Technology, Tehran, Iran
e-mail: nas_moghaddas@kntu.ac.ir

Many researchers investigated the beneficial ability of cellular geosynthetic mattress constructions, called "geocells-reinforced beds", to improve the bearing capacity and settlement of footings (Yang et al. 2012; Moghaddas Tafreshi et al. 2015; Tavakoli Mehrjardi et al. 2012, 2013, 2015; Avesani Neto et al. 2015; Hegde and Sitharam 2015; Aboobacker et al. 2015; Biabani et al. 2016; Kumar and Saride 2016; Sireesh et al. 2016). Rajagopal et al. (1999) investigated the influence of geocell confinement on the strength and stiffness behavior of granular soils through a number of triaxial compression tests. Latha et al. (2006) and Latha and Murthy (2007) conducted a series of compression tests to study the relative efficiency of three forms (i.e. planar, discrete fiber and cellular forms) of reinforcement in improving the shear strength of sand. They investigated that the cellular reinforcement, which improved the strength of soil by friction and all-round confinement, was found to be more effective in improving the soil strength than the planar reinforcement. Zhou and Wen (2008) also observed that geocell was a superior form of reinforcement than the planar reinforcement through triaxial compression tests. The results from their study also indicated that with the provision of a geocell-reinforced sand cushion, the subgrade reaction coefficient was improved by three times, and the deformation was reduced by 44%. Dash et al. (2001, 2003, 2007) investigated the reinforced performance of geocell foundation mattress with varying cell sizes, infill material properties, and loading conditions. They found that the effectiveness of the reinforcement depended not only on the adequate load transmission to the fill material (via friction and interlocking) but also on the stiffness of the reinforcement.

4.2   Failure Mechanisms

Based on experiments of various researchers, four types of failure mechanisms are observed in planar reinforcement according to Figs. 4.1, 4.2, 4.3, and 4.4:

(a) Failure above the upper reinforced layer according to Fig. 4.1 (Binquet and Lee 1975),
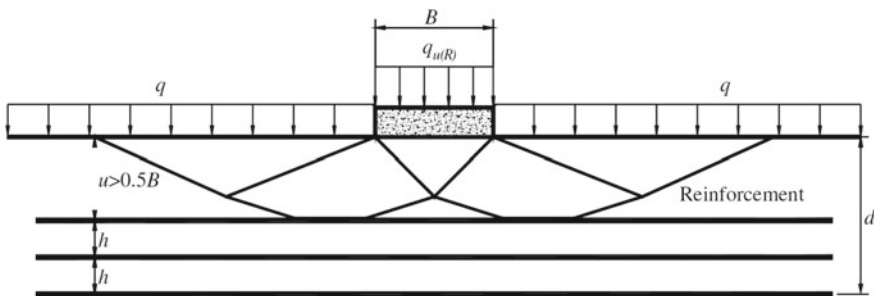(b) Failure between reinforced layers according to Fig. 4.2 (Wayne et al. 1998),

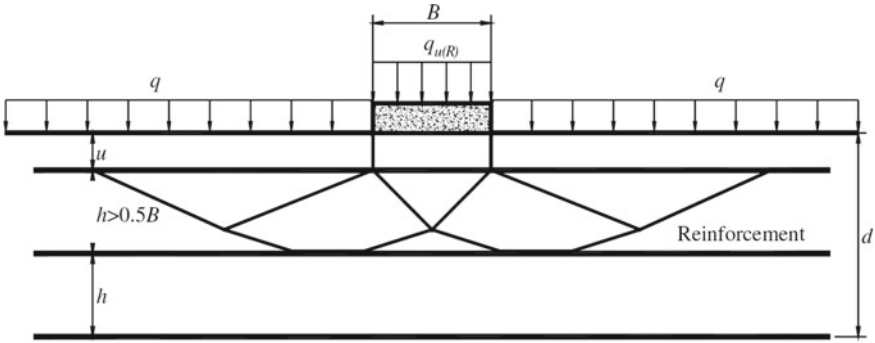**Fig. 4.1** Failure above the upper reinforced layer (Binquet and Lee 1975)

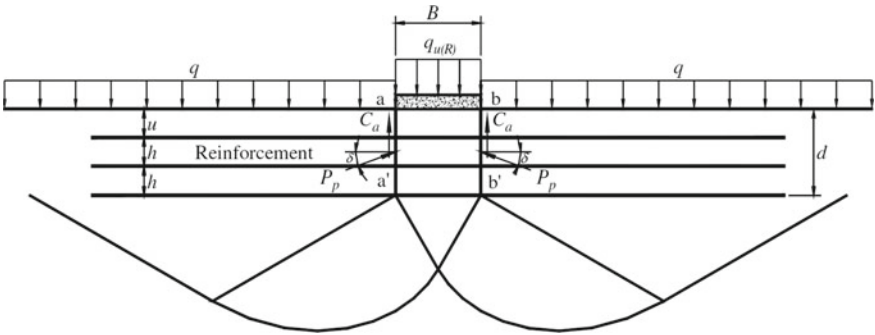**Fig. 4.2** Failure between reinforced layers (Wayne et al. 1998)

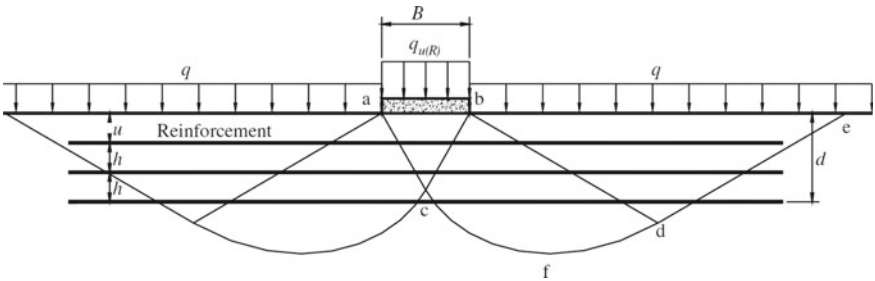**Fig. 4.3** Failure similar to footings on a two-layered soil (Wayne et al. 1998)

Fig. 4.4 Failure inside the reinforced zone (Sharma et al. 2009)

(c) Failure similar to footings on a two-layered soil (strong layer placed on weak layer) according to Fig. 4.3 (Wayne et al. 1998),

(d) Failure inside the reinforced layer according to Fig. 4.4 (Sharma et al. 2009).

According to Figs. 4.1 and 4.2, failures of type (a) and type (b) are most likely to happen when there is excessive distance between the foundation base to the upper

reinforcement layer (*u*) or the distance between reinforcement layers (*h*), presumably when *u* > 0.5*B* or *h* > 0.5*B*. Laboratory studies by Chen et al. (2007) and Abu-Farsakh et al. (2008) shows that to prevent these types of failures, the distance between the bottom of the footing and the upper reinforcement layer (*u*) and the distance between reinforcement layers (*h*) should be less than half of the footing width (0.5*B*), where *B* is the width the foundation.

According to Fig. 4.3, if the strength of the reinforced zone is much greater than the strength of the underlying unreinforced layer and the depth ratio of reinforcement layers (*d*/*B*) is relatively low, shear punching failure occurs in the reinforced zone, followed by total shear failure in the unreinforced zone. Such a failure mechanism was first suggested by Meyerhof and Hanna (1978) for a strong soil layer placed on a weak soil layer. Wayne et al. (1998) expressed that with minor modifications to the solution by Meyerhof and Hanna (1978), it could be used for calculating the bearing capacity of foundations on reinforced beds.

According to Fig. 4.4, in regular reinforcement status, when the strength of the reinforced zone is slightly larger compared to the underlying unreinforced layer and the values of u and h are smaller than 0.5*B*, the failure occurs inside the reinforcement zone. According to studies by Sharma et al. (2009), the proper type of failure mechanism for clayey and sandy soil are type (c) and type (d), respectively. Separate research experiments by Harikumar et al. (2016) and others on the square footing of a 150 mm dimension on multi-directional reinforcing elements reported the optimum embedment depth of 0.5*B*. 1.3% increase in bearing capacity and 0.72% reduction in the settlement were obtained by embedding the reinforcement layer at depth of 0.5*B* compared to unreinforced beds. Based on the height of geocell, the distance between geocell layers and stiffness of soil layers, these failure mechanisms can be extended to geocell-reinforced systems, which need further investigation to obtain the exact limits for the influencing factors.

Zhao et al. (2009) reviewed the response of geocell-reinforced layers under embankments and suggested the three aspects of main geocell layer functions, including (a) vertical stress dispersion effect, (b) membrane effect, and (c) lateral resistance effect, which are explained briefly as the follows:

(a) *Vertical stress dispersion effect*

The horizontal geocell-reinforced cushion behaves as an immediate working platform that redistributes the footing load per unit area over a wider area, as shown in Fig. 4.5. This refers to herein as "stress dispersion effect". As a result, the soil pressure onto the soft subgrade soil surface is smaller than that onto the subgrade soil in the absence of geocell.

As far as the applied surface stress can be distributed based on the 2:1 method in the unreinforced foundation, Tavakoli Mehrjardi et al. (2015) proposed that, in geocell-reinforced foundation, the stress can be considered to be longitudinally distributed on an equivalent circle with diameter "*D*" as per Eq. (4.1).
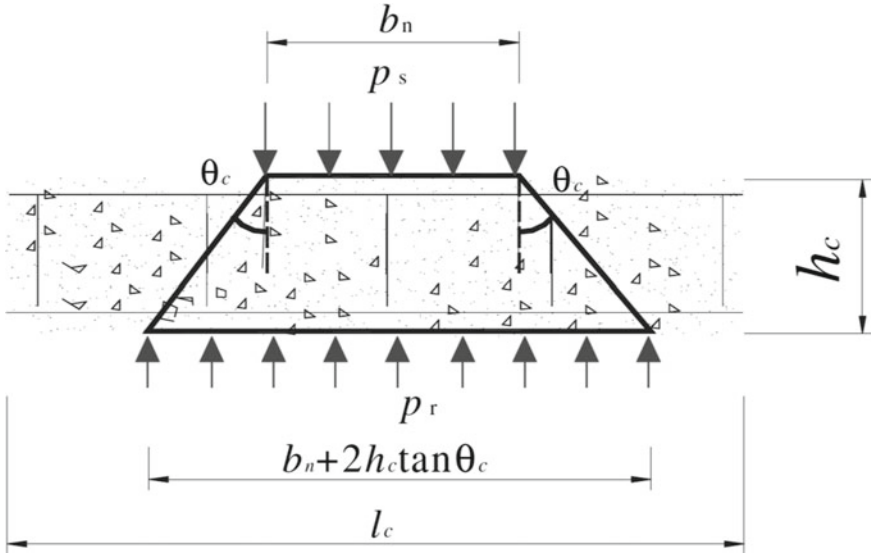
$$D = B + nH \tag{4.1}$$

Fig. 4.5 Vertical stress dispersion effect of geocell reinforcement (Zhang et al. 2010a, b)

where

B Footing width
H considered depth of the foundation
n load spreading factor which ≈ 1.5.

(b) ***Membrane effect***

The loads from the embankment deflect the geocell reinforcement generating a further tension force, as shown in Fig. 4.6. The vertical component of the tension force in the reinforcement is helpful to reduce the pressure on the subgrade soil. Then, the vertical deformation of the soft subgrade is reduced and the bearing capacity of the subgrade soil is enhanced as well. In tandem with increasing the surface settlement, the geocell layer deformed more, bringing about a further tension force due to this membrane effect.
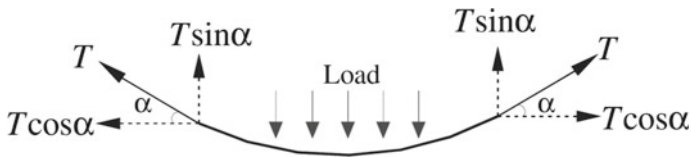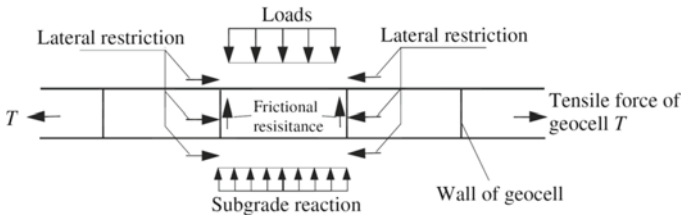
(c) **Lateral resistance effect**

Fig. 4.6 Membrane effect of geocell reinforcement (Zhang et al. 2010a, b)

Fig. 4.7 Lateral resistance effect of geocell reinforcement (Zhang et al. 2010a, b)

Geocells consist of three-dimensional cells containing the filled materials, causing lateral spreading which, in turn, results in improving the shear strength of filled materials. Moreover, interfacial resistances, which result from the interaction between the geocell reinforcement and the soils below and above the reinforcement, as shown in Fig. 4.7, increase the lateral confinement and lower lateral strain, that results in an increase in the modulus of the cushion layer and improving vertical stress distribution on the subgrade which is called "vertical stress dispersion effect" reducing the vertical pressure on the top of the subgrade, correspondingly.

Since anchorage and/or tensioned membrane effects of geocells are predominantly influenced by the mobilized shear strength at the geocells–soil interface, therefore in the load support applications, the interfacial properties of geocell-reinforced soil should be determined. In this regard, Tavakoli Mehrjardi and Motarjemi (2018) carried out a series of large direct shear test to investigate the interactive parameters of geocell-soil composite on the interface's shear strength with respect to the backfill aggregate size. In this study, geocells made of a tape of Heat-Bonded Nonwoven geotextile (HBNW) had the pocket size and height of 55 mm × 55 mm and 50 mm, respectively. Moreover, two relative densities of fill materials (50 and 70% which represent medium dense and dense backfill, respectively), three aggregate sizes of fill materials (3, 6 and 12 mm–selected based on the scaling criteria on size of shear box and geocell pockets), and three normal stresses (100, 200 and 300 kPa—these values cover rather low to high vertical stress in a soil element of common geotechnical projects) have been examined.

To have a shortcut to the results observed in the study, Table 4.1 is presented. This table summarizes the influences of all studied parameters on the interfacial characteristics of grains-grains (unreinforced status) and grains-geocell (reinforced status) interactions. In way of illustration, Table 4.1 states that an upward trend of *medium grain size of fill materials improved both friction angle and cohesion mobilized at the interface, regardless of the reinforcement* statuses *(Tavakoli Mehrjardi and Motarjemi 2018). Further results can be summarized as follows*:

– Unlike the positive effect of geocell, the normal stress had a negative influence on the advancement of dilation angle, tending to reduction in the beneficial effect of the grains size increment on the improving interface's shear strength. Therefore, using geocells in low normal stress and large main particle size is more recommended.

**Table 4.1** Properties of all three soils used in the tests

Parameters	Reinforcement Status	τ_{max}	τ_{cv}	ϕ	c	ψ
Relative density	Unreinforced	↑	↑	↑	← in $D_{50} = 3$ and 6 mm cte. in $D_{50} = 12$ mm	↑
	Reinforced	← in $D_{50} = 3$ and 6 mm → in $D_{50} = 12$ mm	↓	← in $D_{50} = 3$ mm cte. in $D_{50} = 6$ and 12 mm	← in $D_{50} = 3$ and 6 mm → in $D_{50} = 12$ mm	↑
Normal Stress	Unreinforced	↑	↑	↓	↑	↓
	Reinforced	↑	↑	↓	↑	↓
medium Grain Size	Unreinforced	↑	↑	↑	↑	↑
	Reinforced	↑	↑	↑	↑	↑
Geocell reinforcement	Reinforced	↑	↑	Cte. (excepted from large grains at low relative density)	↑	↑

Tavakoli Mehrjardi and Motarjemi (2018)

↑← mean increase and ↓→ mean decrease

– For medium dense fill materials, increasing soil particle size strengthens the beneficial role of the geocell and improved stability of the materials after reaching the shear strength at peak. On the contrary, the advancement of relative density and normal stress, to some extent, reduced the geocell efforts in increasing the shear strength of the interface.
– For coarse aggregates (cell aspect ratio smaller than 8.5), the geocell reinforcement was more efficient, in the order of two times, at least, more than compaction effort in the enhancement of shear characteristics mobilized at the interface.
– *geocell reinforcement had no significant effect on interface's friction angle at high relative density.*
– geocells mobilize an apparent cohesion on the shear interface owing to the provision of some confinement for the aggregates located in the neighbor of the shear plane. For geocell-reinforced samples with $D_r = 50\%$, the apparent cohesion has substantially increased by about 1.9–23 kPa.
– The results clarify that among the studied variables, geocell with cell aspect ratio [the ratio of the geocell's cells size (b) to the medium grains size (D_{50})] 4 has the best performance in the improvement of interface's shear strength.

Moreover, to observe the effective parameters on the shear characteristics of geocell–grains interface, Fig. 4.8 is illustrated. From this figure, during shearing, interlocking effect which mobilizes apparent cohesion and friction at the interface,
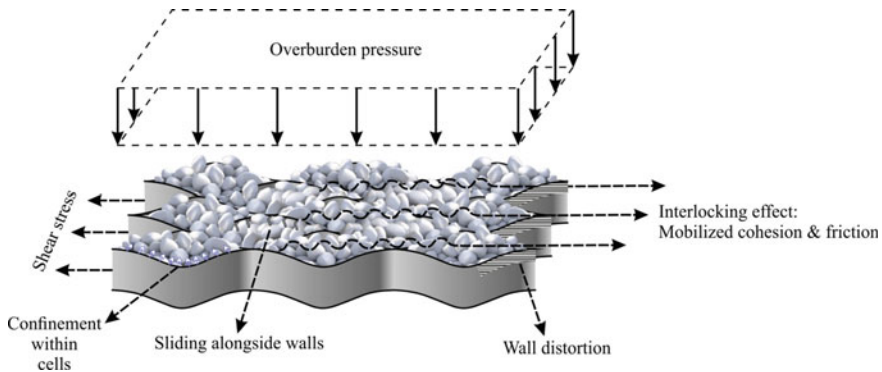
Fig. 4.8 Sketch of effective parameters on the shear characteristics of geocell–grains interface (Tavakoli Mehrjardi and Motarjemi 2018)

besides the confinement effect on grains within the geocell's cells, producing interface's shear strength. Based on the acquired results, it was found out that shear strength of the interface encountered weakness in the aftermath of grain sliding alongside the geocell's walls and also, geocell's walls distortion.

If the mentioned failure mechanisms of the geocell-reinforced bed include the layers of geocell, then the geocell has ruptured. The ruptured geocells can exhibit failure modes related to the junction welds between geocell strips. A series of tests were performed by Liu et al. (2019) on HPDE geocell to recognize possible failure modes of the junctions. According to the tensile tests, two failure modes were identified for geocell junctions under tensile loading, which can be observed in Fig. 4.9b, c. All specimens experienced identical behavior in their initial stage of failure, with the elongation initiating from approximately the middle of the welds, as shown in Fig. 4.9a. The initial stage was then followed by two different failure modes. Some specimens continued elongating in a vertical manner until rupture occurred (Fig. 4.9d). Whereas, for others, the fracture was initiated from the left-hand side after reaching its peak tensile strength and followed by rupture which propagated towards the right-hand edge. Similar failure modes were observed on the cell-wall which was attributed to the stress concentration caused by inconsistent indentation depths.

Regarding shearing, all specimens experienced similar failure modes, where the rupture occurred adjacent to the junction, as shown in Fig. 4.10. This indicates that the junction is unlikely to fail during shearing and the shear strength of the junction is significantly higher than the peak shear stresses obtained from the present experimental program, yet it is more vulnerable to tensile stress. This observation is confirmed by the elongation mode in Fig. 4.10b, where the specimen deformed only in the cell-wall strip, while the junction remained intact.

Under the action of peeling, two failure modes were observed, as are shown in Fig. 4.11. Only one of the five tested specimens experienced weld fracture (Fig. 4.11c), while the other specimens failed in the cell-wall adjacent to the
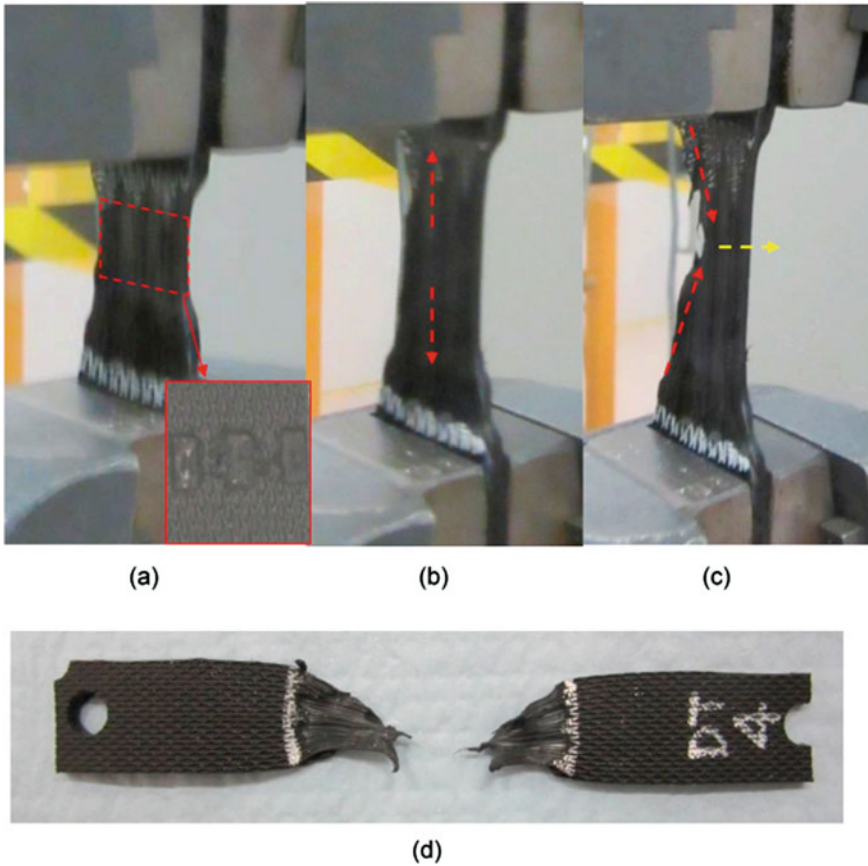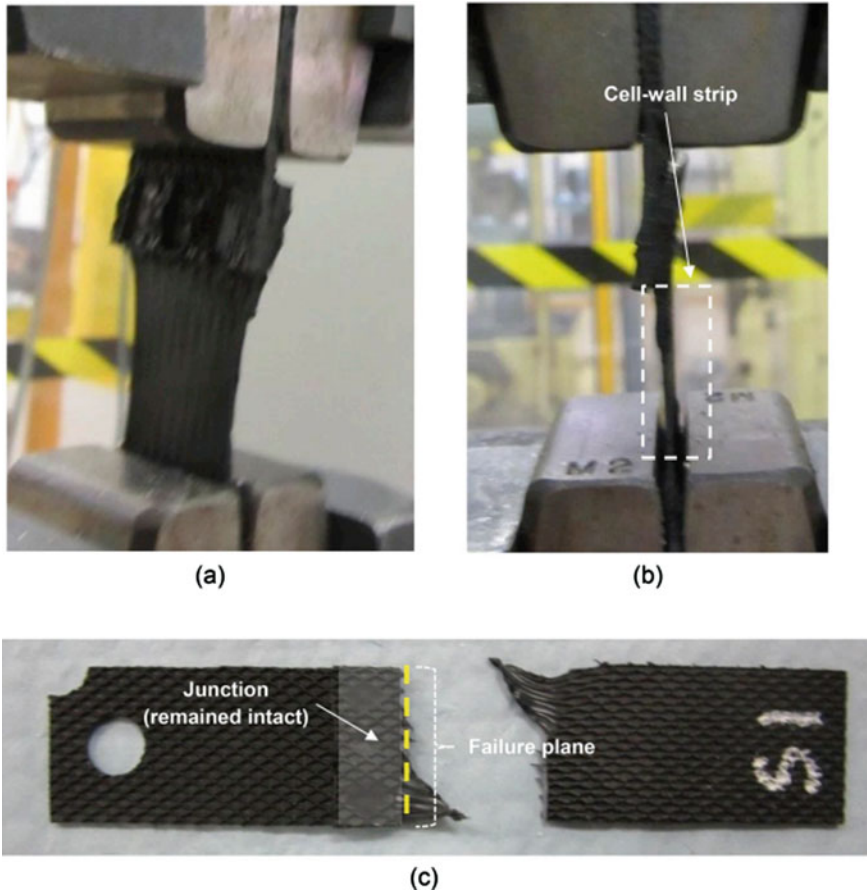
Fig. 4.9 Failure modes of the geocell junction subjected to uniaxial tension: **a** initial stage (pre-peak), **b** failure mode 1 (post-peak), **c** failure mode 2 (post-peak), and **d** ruptured specimen (Liu et al. 2019)

weld junction (weld failure). This specimen also experienced the most fluctuations throughout the loading process. Due to the low possibility of occurrence of this failure mode, it is considered that this is likely the result of faulty/unsatisfactory welding during manufacturing.

Unlike other loads, which occur less frequently when the geocell is placed in the field, such as in the case of pavement or slopes, the junctions are constantly subjected to a splitting force. Two types of failure mechanisms were observed, as shown in Fig. 4.12. The failure mode is shown in Fig. 4.12b can be described as occurring when the two welded, cell-wall strips completely separated from each other due to the rupture of the weld. The failure mode being shown in Fig. 4.12c is defined as cell-wall failure, as the junction did not fail under the influence of the splitting force. The latter mode is similar to the failure condition under shearing and peeling.
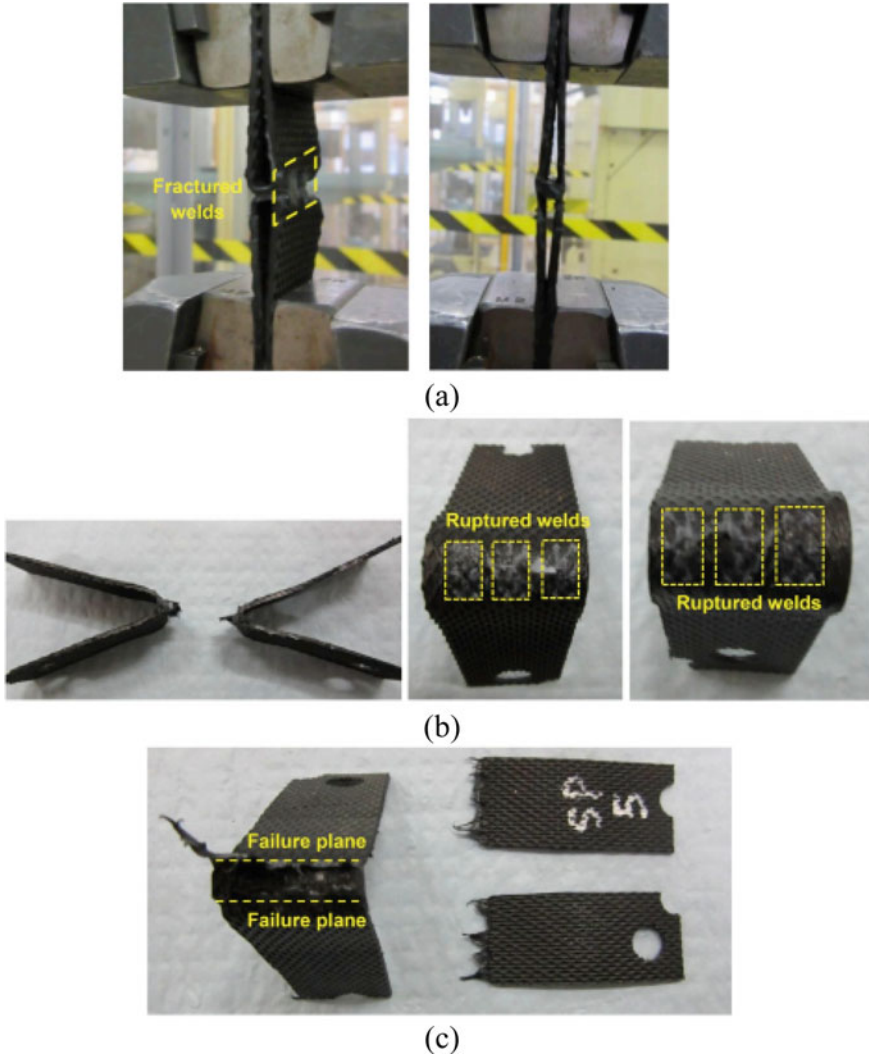
Fig. 4.10 Failure modes of geocell junctions subjected to shear force: **a** oblique view and **b** side view during testing, and **c** failed specimen (Liu et al. 2019)

It should be noted that geocell junctions exhibit a higher splitting strength when the junctions experience the failure mode of complete separation. As the stress–displacement relationship was obtained from the seam strength tests, the geocell junctions reached their peak strength under the splitting load, significantly slower than in other loading scenarios. This phenomenon suggests that when geocells are used in the field (such as in slope protection), it is possible that the soil structure will experience a gradual down-slope movement prior to failure if the gravitational load exceeds that specified by the manufacturer. The post-peak behavior suggests that, once the junction reaches its splitting strength, failure occurs faster when compared with other loading conditions.
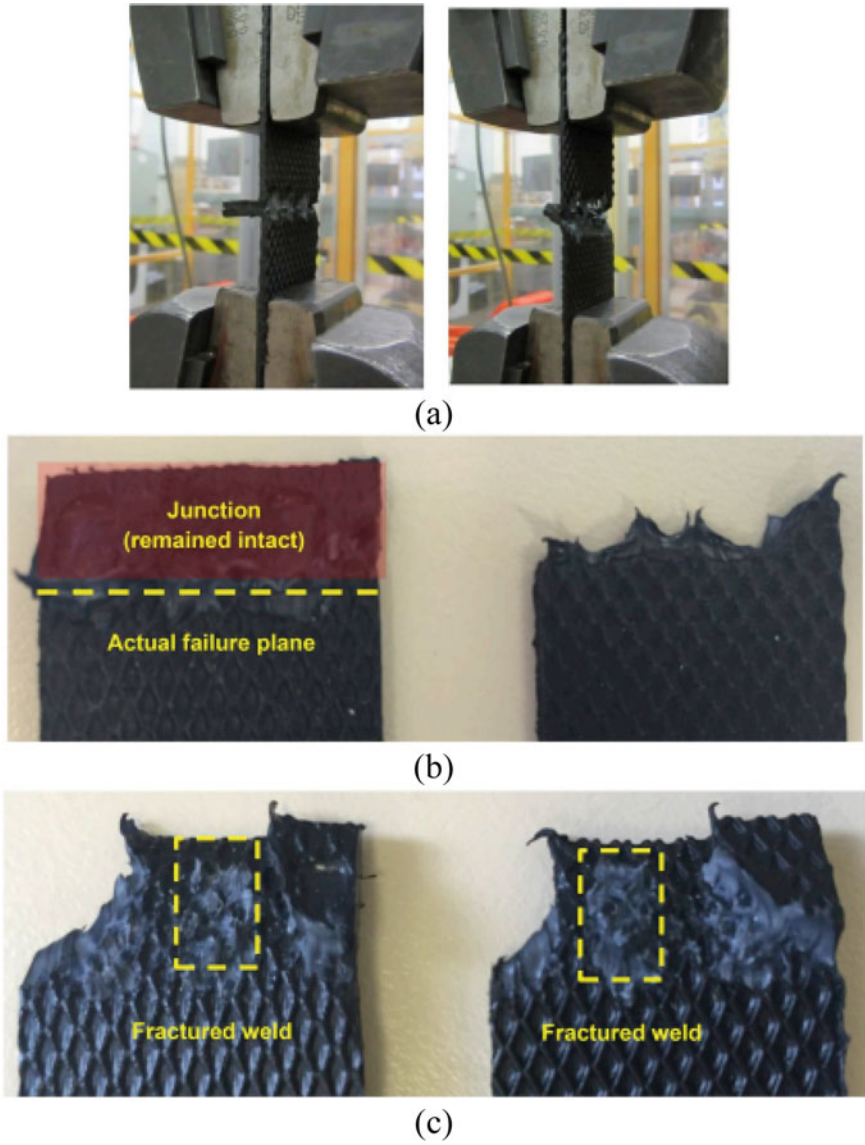
Fig. 4.11 Failure modes of geocell junctions subjected to peeling force: **a** during testing, **b** strip failure, **c** weld failure (Liu et al. 2019)

Fig. 4.12 Failure modes of geocell junctions subjected to a splitting force: **a** during testing; **b** junction failure; **c** cell-wall strip failure (Liu et al. 2019)

4.3 Equating the Response of Geocell-Reinforced Foundations

Limited works have been done on the design of road embankment supported by geocell-reinforced cushion. Jenner et al. (1988) used a slip line theory to calculate the increase in the bearing capacity of soft soil due to the provision of geocell cushion at the base of the embankment. In their method, plastic bearing failure of the soil was

assumed and the additional resistance due to geocell layer was calculated using a non-symmetric slip line field in the soft subgrade soil. This method was very complicated as it needed to construct a slip line field for every embankment problem. Koerner (1998) presented a bearing capacity calculation method by adapting the conventional plastic limit equilibrium mechanism as used in statically loaded shallow foundation bearing capacity. In his method, the shear strength between geocell wall and soil contained within it was considered as a bearing capacity increment on the foundation soil due to the presence of the geocell reinforcement at the base of the embankment. Latha et al. (2006) proposed a method to design the geocell-supported embankments based on the study of laboratory model tests. The method was based on the slope-stability analysis, and the critical slip surfaces of embankments should be checked by the slope-stability program for every design. In their analysis, the geocell layer was treated as a foundation soil layer with additional cohesive strength caused by confinement.

In this section, relevant equations for the response of geocell-reinforced foundations including bearing capacity and the corresponding settlements are presented.

4.3.1 Single-Layered Geocell-Reinforced Foundation

Zhang et al. (2010a, b) propose a simple bearing capacity calculation method for the geocell-supported embankment over soft soil, with consideration of the main reinforcement functions of geocell layer studied above. In this study, the bearing capacity of geocell-reinforced foundation "p_{rs}" is estimated by putting the bearing capacity of the untreated foundation soil "p_s" and the bearing capacity increment "Δp" on the foundation soil due to the presence of the geocell-reinforced cushion together. The methods to determine "p_s" have been developed or proposed correspondingly in the literature (Lambe and Whitman 1969). It can be determined by empirical values or equations, or site load testings.

As discussed beforehand, the main reinforcement mechanisms of the geocell in embankment engineering are "lateral resistance effect", "vertical stress dispersion effect" and "membrane effect". Generally, the effect of lateral resistance of geocell reinforcement is mostly related to the resistance against the lateral deformations of embankments. So, the lateral resistance effect of geocell reinforcement has no direct effect on increasing the bearing capacity of the subgrade soil. The bearing capacity increment "Δp" on the foundation soil can be made up of two aspects, notably the bearing capacity increment "Δp_1" due to the "vertical stress dispersion effect", and the bearing capacity increment "Δp_2" due to the "membrane effect" of the geocell reinforcement.

According to Fig. 4.6, the geocell-reinforced cushion widens the spreading of vertical stress so that, in turn, the subgrade soil can support more upper loads than that without geocell-reinforced cushion. The footing load per unit area increases from "p_s" to "p_r", according to Eq. (4.2).

$$p_r = \frac{(b_n + 2h_c \tan \theta_c)}{b_n} p_s \qquad (4.2)$$

where "p_r" is the footing load due to the vertical stress dispersion effect; "b_n" is the width of the uniform load "p_s", as shown in Fig. 4.6; "h_c" and "θ_c" are the height and the dispersion angle of geocell reinforcement, respectively. Thus, the bearing capacity increment "Δp_1" by the "vertical stress dispersion effect" can be calculated as Eq. (4.3).

$$\Delta p_1 = p_r - p_s = \frac{2h_c \tan \theta_c}{b_n} p_s \qquad (4.3)$$

As shown in Fig. 4.7, the bearing capacity increment "Δp_2" on the foundation soil due to the tensile force of the geocell reinforcement can be estimated as Eq. (4.4).

$$\Delta p_2 = \frac{2T \sin \alpha}{b_n} \qquad (4.4)$$

where "T" is the tensile force of the reinforcement and can be calculated from Eq. (4.5).

$$T = E_c \varepsilon h_g \qquad (4.5)$$

where "E_c" is the tensile modulus of the geocell material and can be estimated by an indoor tensile test (ASTM D638-14); "ε" is the tensile strain of the geocell material; "h_g" is the height of the geocell wall; "a" is the horizontal angle of the tensional force "T".

Before calculating "ε", the deformation shape of the reinforcement should be determined. Sophisticated numerical analyses have shown that the shape of the deflected geocell is a catenary (BS8006 1995; Yin 2000). However, at relatively small deflections the catenary may be approximated by a parabola which simplifies the analysis procedure for determining the tensile force in the geocell. As shown in Fig. 4.13, the deformation on the road surface is in the form of Eq. (4.6).

$$y_0 = -\frac{\Delta_0}{r_0^2} x^2 + h_0 + \Delta s_0 \qquad (4.6)$$

where "y_0" is the deformation on the road surface; "Δs_0" is the maximum differential settlement at the surface; "h_0" is the vertical distance from the origin of coordinates shown in Fig. 4.13 to the embankment surface. By differentiating Eqs. (4.5) and (4.7) is obtained.

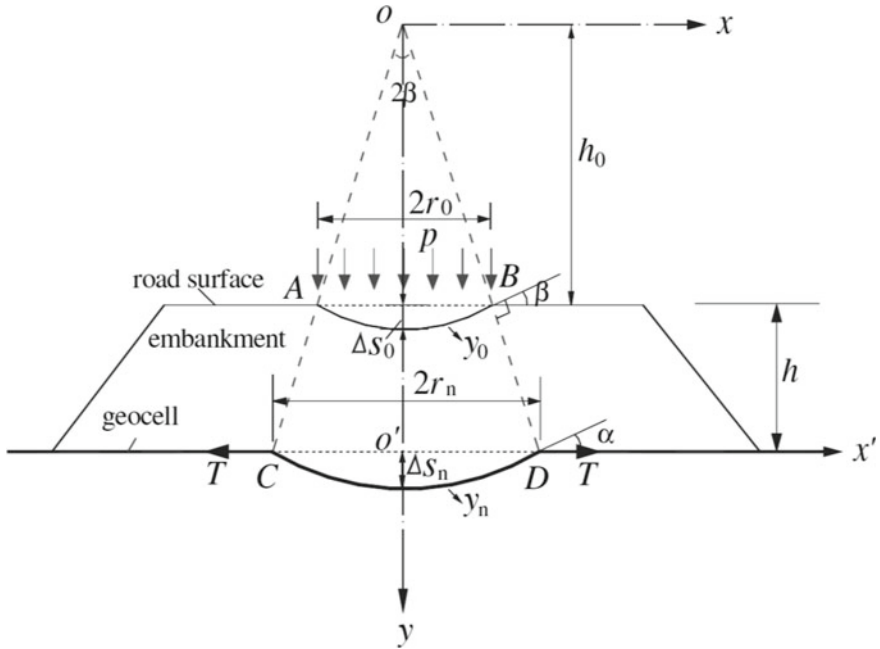$$\frac{dy_0}{dx} = -\frac{2\Delta s_0}{r_0^2} x \qquad (4.7)$$

Fig. 4.13 Calculation model of the geocell-reinforced embankment (Zhang et al. 2010a, b)

When $x = r_0$, $dy_0/dx = -2\Delta s_0/r_0$. Supposing that the normal directions of points A and B on the deformation parabola are the same as the diffusion directions of embankment fill under the external load "p", then, Eq. (4.8) can be presented.

$$\tan \beta = \frac{2\Delta s_0}{r_0} = \frac{r_0}{h_0} = \frac{r_n}{h_0 + h} \tag{4.8}$$

where "b" is the angle depicted in Fig. 4.13; "r_n" is the half of the chord length of parabola depicted in Fig. 4.13 and calculated by Eq. (4.9); "h" is the height of the embankment.

$$r_n = \frac{r_0^2 + 2\Delta s_0 h}{r_0} \tag{4.9}$$

The relative deformation equation of the geocell reinforcement shown in Fig. 4.13 is in the form of Eq. (4.10).

$$y_n = -\frac{\Delta s_n}{r_n^2}x^2 + h_0 + h + \Delta s_n \tag{4.10}$$

where "y_n" is the deformation of the geocell reinforcement; "Δs_n" is the maximum vertical deformation of the reinforcement. Be similar to Eqs. (4.6) and (4.11) is

obtained.

$$\sin \alpha = \left[1 + \left(\frac{r_n}{2\Delta s_n} \right)^2 \right]^{-\frac{1}{2}} \tag{4.11}$$

Then, the tensile strain of the geocell (ε) is determined as Eq. (4.12).

$$\varepsilon = \frac{1}{2}\delta + \frac{r_n}{4\Delta s_n} \ln\left[\frac{2\Delta s_n}{r_n} + \delta \right] - 1 \tag{4.12}$$

where δ is defined as Eq. (4.13).

$$\delta = \left[1 + \left(\frac{2\Delta s_n}{r_n} \right)^2 \right]^{\frac{1}{2}} \tag{4.13}$$

By the way, the acceptance limit of the tensile strain (ε) is controlled by the ultimate tension strain of the geocell material and the maximum permissible differential settlement of embankment [Δs_0]. Δs_n and Δs_0 follow a relationship as Eq. (4.14).

$$\Delta s_0 = \Delta s_n + \Delta c \tag{4.14}$$

in which, "Δc" is the compression of the embankment material under the load "p". "Δc" can be determined by layer-wise summation method. If the embankment is not very high, "Δc" is nearly zero, and "Δs_n" is close to the differential settlement "Δs_0" on the embankment surface.

As mentioned earlier, the bearing capacity of the geocell-reinforced embankment foundation (p_{rs}) can be evaluated by putting the bearing capacity of the untreated foundation soil (p_s) and the bearing capacity increment (Δp) on the foundation soil due to the placement of the geocell-reinforced cushion at the base of the embankment together, leading to Eq. (4.15).

$$p_{rs} = p_s + \Delta p = p_s + \Delta p_1 + \Delta p_2 = p_s + \frac{2h_c \tan \theta_c}{b_n} p_s + \frac{2T \sin \alpha}{b_n} \tag{4.15}$$

Depending on what aspects of failure mechanisms for geocell-reinforced foundation had been considered, other researchers have presented relationships for other forms of bearing capacity, summarized in Table 4.2. In all equations:

p_r bearing capacity of geocell-reinforced foundation (kPa),
δ interface shear angle between the cell-wall and the filling soil (°),
k_0 coefficient earth pressure at rest,
p_u bearing capacity of unreinforced soil (kPa),
h/d geocell aspect ratio,
p applied pressure on the geocell mattress (kPa),

B   width of the applied pressure system (m).

## 4.3.2 Multi-layered Geocell-Reinforced Foundation

For a semi-infinite soil medium of the elastic modulus E_n and Poisson's ratio v_n, subjected to uniform pressure q on a circular footing with radius a, the immediate settlement at the depth z below the center of flexible footing is written as Eq. (4.16) (Harr 1966). Equation (4.16) is valid for a flexible footing and should be multiplied by $\pi/4$ for a rigid footing.

$$w(z) = \frac{2aq\left(1 - v_n^2\right)}{E_n}\left(\sqrt{1 + \frac{z^2}{a^2}} - \frac{z}{a}\right)\left\{1 + \frac{z/a}{2(1 - v_n)\sqrt{1 + \frac{z^2}{a^2}}}\right\} \qquad (4.16)$$

Hirai (2008) developed the elastic relationships of multi-layer soil stiffness modulus. Figure 4.14 shows a multi-layered soil system composed of *n*-layers of soil subjected to vertical loads *q*. As shown in Fig. 4.14, the present procedure uses the elastic moduli, i.e., Young's modulus of E_m, Poisson's ratio of v_m and thickness of H_m for *m*th layer in *n*-layers of multi-layered soil system. Parameters D and D_f are the diameter and embedment depth of a footing, respectively. The *n*-layered soil system shown in Fig. 4.14 was transformed into an equivalent two-layered soil system illustrated in Fig. 4.15a. The equivalent elastic modulus of E_H (Hirai and Kamei 2003, 2004) for $(n - 1)$ layers in Fig. 4.15a (where $H = H_1 + H_2 + H_3 + \cdots + H_{n-1}$) was represented by Eq. (4.17).

Fig. 4.14 Multi-layered soil systems (Hirai 2008)
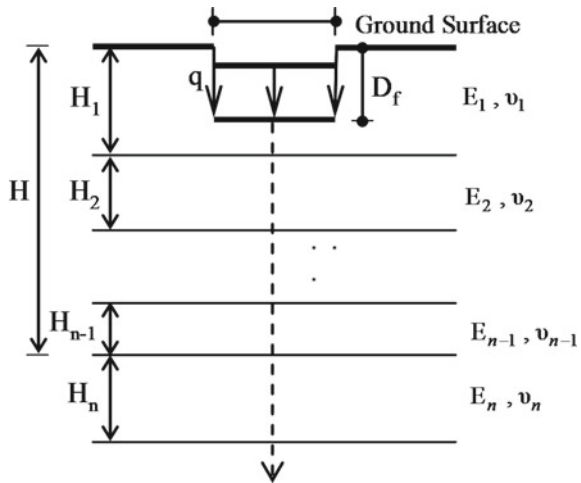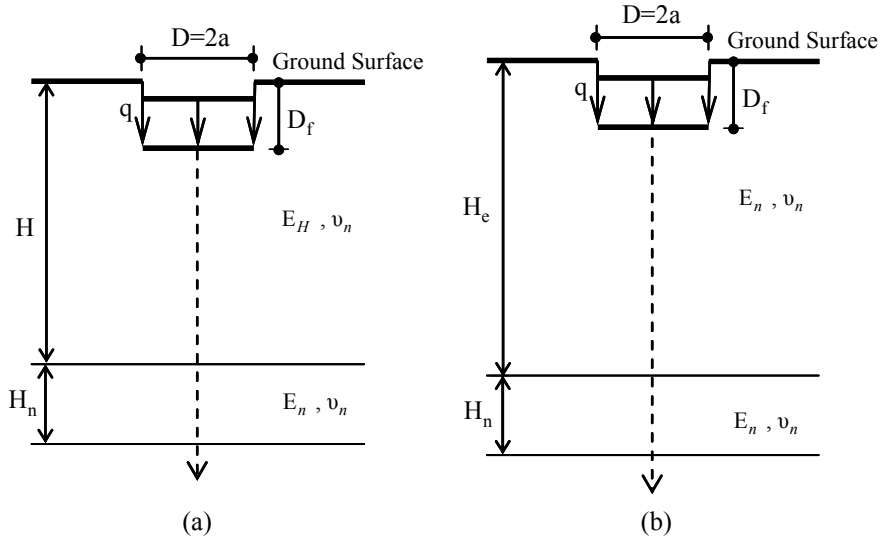
Fig. 4.15 **a** Equivalent two-layered soil system for Fig. 4.14, and **b** Equivalent single-layer soil system with the same E_n and v_n for Fig. 4.15a (Hirai 2008)

$$E_H = \left[\left\{ E_1 \frac{(1-v_n^2)}{(1-v_1^2)} \right\}^{\frac{1}{3}} \frac{H_1 - D_f}{H - D_f} + \sum_{j=2}^{n-1} \left\{ E_j \frac{(1-v_n^2)}{(1-v_j^2)} \right\}^{\frac{1}{3}} \frac{H_j}{H - D_f} \right]^3 \quad (4.17)$$

Next, the two-layered soil system in Fig. 4.15a was transformed into an equivalent single soil layer with an elastic modulus of E_n and Poisson's ratio of v_n, (the thickness of an equivalent single layer is $H = H_e + H_n$) as shown in Fig. 4.15b, using the equivalent thickness relations (4.18) and (4.19) (Hirai and Kamei 2003, 2004; Hirai 2008). For the case where $E_H \geq E_n$:

$$H_e - D_f = \left(\frac{E_H}{E_n} \right)^{1/3} (H - D_f) \quad \text{for } E_H \geq E_n \quad (4.18)$$

$$H_e - D_f = \left[0.75 + 0.25 \left(\frac{E_H}{E_n} \right)^{1/3} \right] (H - D_f) \quad \text{for } E_H \leq E_n \quad (4.19)$$

Likewise, Fig. 4.16 shows an equivalent system of soil layers to that previously illustrated in Fig. 4.14, but now each soil layer has an equivalent thickness of H_{ie} and uniform E and v values for every layer ($=E_n$ and v_n). Thus, the system is reduced to a single-layer system of thickness $H_{1e} + H_{2e} + H_{3e} + \cdots + H_{(n-1)e} + H_n$ and stiffness properties E_n and v_n. The equivalent thickness of each individual layer is required so as to obtain the thinning and strain of each layer of the multi-layered system as it is described later in the current section. According to the Palmer and Barber method

Fig. 4.16 Equivalent single soil layer with equivalent thickness of "$H_{1e} + H_{2e} + H_{3e} + \cdots + H_{(n-1)e} + H_n$" and E_n and v_n for Fig. 4.14 (Hirai 2008)
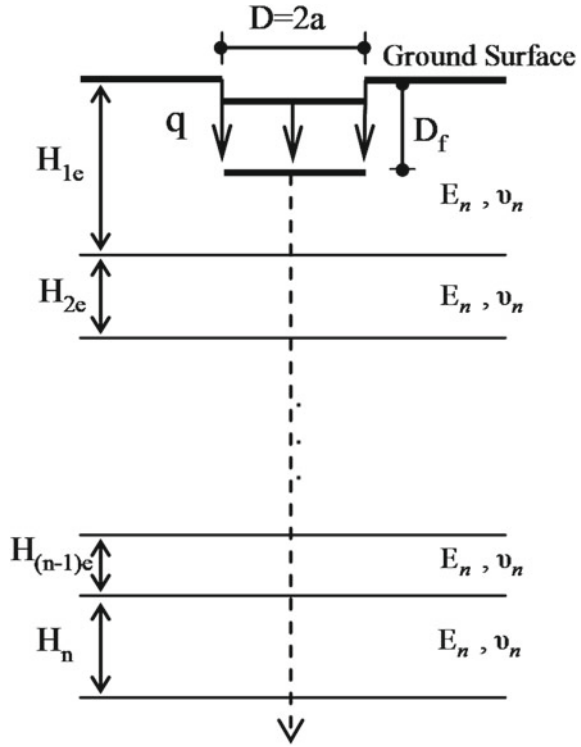
(1940) for a two-layer system and to Odemark's method (1949) for a multi-layered soil system, Eqs. (4.20) and (4.21), respectively, were derived by Hirai (2008) for estimating the equivalent thickness of each layer for the case where $E_m \geq E_n$.

$$H_{1e} - D_f = \left\{ \frac{E_1(1 - v_n^2)}{E_n(1 - v_1^2)} \right\}^{1/3} (H_1 - D_f) \tag{4.20}$$

$$H_{me} = \left\{ \frac{E_m(1 - v_n^2)}{E_n(1 - v_m^2)} \right\}^{1/3} H_m (m = 2 \sim n) \tag{4.21}$$

For the case where $E_m \leq E_n$, by considering Terzaghi's approximate formula (1943), the equivalent thickness is given by Eqs. (4.22) and (4.23).

$$H_{1e} - D_f = \left[0.75 + 0.25 \left\{ \frac{E_1(1 - v_n^2)}{E_n(1 - v_1^2)} \right\}^{1/3} \right] (H_1 - D_f) \tag{4.22}$$

$$H_{me} = \left[0.75 + 0.25 \left\{ \frac{E_m(1 - v_n^2)}{E_n(1 - v_m^2)} \right\}^{1/3} \right] H_m \, (m = 2 \sim n) \qquad (4.23)$$

where H_{1e} and H_{me} are the values of H_e for the first and subsequent layers ($m = 2$ to n), respectively, and E_1, v_1, E_n, v_n and E_m, v_m are values of E_H and v for layers 1, n and $m = 2$ to n, respectively.

$$w_1 = \frac{2aq\left(1 - v_n^2\right)}{E_n} \left(\sqrt{1 + \left(\frac{H_e}{a}\right)^2} - \frac{H_e}{a} \right) \left(1 + \frac{H_e}{2a(1 - v_n)\sqrt{1 + \left(\frac{H_e}{a}\right)^2}} \right)$$
$$(4.24)$$

Vakili (2008) developed the method of Foster and Ahlvin (1959) to evaluate the surface settlement of the equivalent system shown in Fig. 4.16. According to this method, the actual vertical surface deflection of a footing (w) was obtained by adding the amount of thinning, w_2, of the equivalent layer (with thickness of H_e) between the surface ($z = 0$) and a depth of $z = H_e$ to the vertical deflection at a depth of $z = H_e$ of a semi-infinite mass below that depth (i.e. deflection of w_1 at bottom of the equivalent layer). In the case of uniform pressure "q" on a flexible circular footing with radius "a" (Fig. 4.14), supported by a semi-infinite mass, w_1 is obtained by substituting the value of $z = H_e$ from Eq. (4.18)/ or Eq. (4.19) into Eq. (4.16) to obtain Eq. (4.24).

Similarly, the vertical deflection at the center of loading on the surface (i.e. w_0 at depth of $z = 0$) of uniform equivalent layer (i.e. for the footing on the equivalent layer), substituting the value of $z = 0$ into Eq. (4.16) results in Eq. (4.25).

$$w_0 = \frac{2a\left(1 - v_n^2\right)q}{E_n} \qquad (4.25)$$

Equations (4.24) and (4.25) are valid for a flexible footing and should be multiplied by $\pi/4$ for a rigid footing. The vertical thinning of the equivalent layer [with thickness of H_e as in Fig. 4.15b) between the loading surface ($z = 0$) and a depth of $z = H_e$ (i.e. ($w_0 - w_1$)], can be converted to the thinning, w_2, of the original layer (thickness H as in Figs. 4.14 and 4.15a), using Eq. (4.26).

$$w_2 = \frac{E_n}{E_H}(w_0 - w_1) \qquad (4.26)$$

Hence, Eqs. (4.24) and (4.26) may be summed to obtain the actual total surface settlement of the circular footing ($w = w_1 + w_2$).

Moghaddas Tafreshi et al. (2015) presented a new analytical solution, based on the theory of multi-layered soil system to estimate the pressure-settlement response of a circular footing resting on multi-layered geocell-reinforced foundation comprising non-cohesive soil.

The "n"-layered soil system theory (Hirai 2008) and surface settlement of equivalent system (Vakili 2008) were employed to evaluate the pressure-settlement of footings supported by a multi-layer geocell-reinforced bed as shown in Fig. 4.17. This figure shows a schematic model of a shallow circular footing with diameter, $D = 2a$, located on a typical n-layer foundation bed composed of "m" geocell layers and "$n - m$" soil layers, under the application of a uniformly distributed surface load, q. The thicknesses of geocell and soil layers are h_g and h_s, respectively. The first geocell layer is placed at a depth of u beneath the footing and the remaining geocell layers are located after an unreinforced soil thickness of h_s. The effective depth, H_{eff}, is assumed as the depth to a point below the footing at which only 10% of the applied stress on footing surface acts. The elastic modulus, E_i, and Poisson's ratio, v_i ($i = 1, 2, 3, …, n$) of each layer is as given in Fig. 4.17. H_{n-1} is the thickness of the $(n - 1)$th layer which can be calculated using Eq. (4.27).

$$H_{n-1} = H_{\text{eff}} - u - mh_g - (m-1)h_s \qquad (4.27)$$

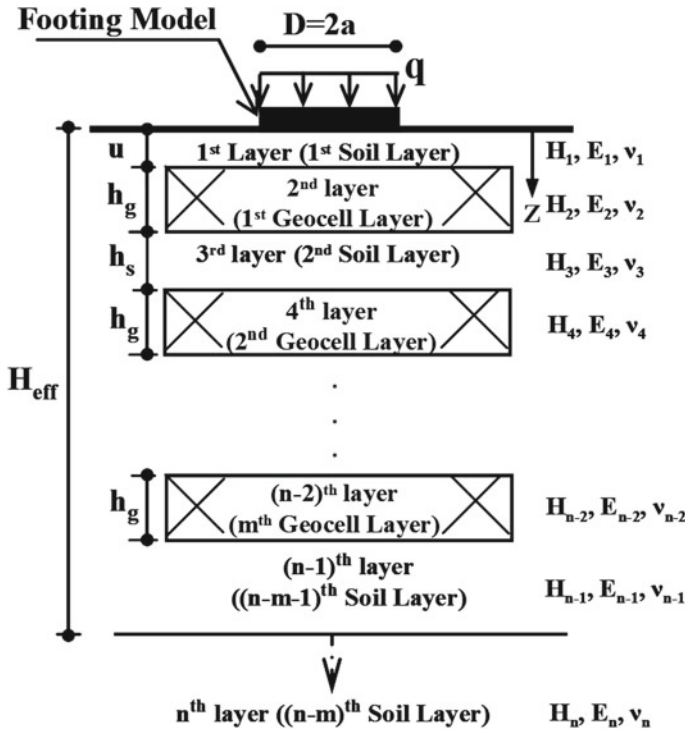Beforehand, it should be mentioned that the following simplifying assumptions are made in this analysis, as follows:

Fig. 4.17 "n" layer geocell-reinforced soil system containing "m" layers of geocell (Moghaddas Tafreshi et al. 2015)

- The soil layers are homogeneous, isotropic and non-cohesive;
- The unreinforced and reinforced layers deform only in the vertical direction;
- The footing is circular with no embedment depth, $D_f = 0$;
- The behavior of unreinforced and reinforced layers is assumed to be nonlinear elastic;
- Poisson's ratio is assumed to be in the range 0.2–0.3 (see below).

It is known that geocell layers don't expand much horizontally once properly filled with granular soil and compacted (Dash et al. 2007; Pokharel 2010). Thus, the proposed analytical model does not directly consider lateral deformation but, instead, allows for some, indirectly, by using:

(1) Elasticity moduli of the soil and geocell-reinforced layers that were obtained from calibration of the proposed equations (presented later in this section) to the data obtained in the triaxial test that included some lateral deformation, and

(2) Poisson's ratio values of 0.2–0.3, for the unreinforced and geocell-reinforced layers of the foundation bed to compute the equivalent thickness of the multi-layered system, being in line with typical values as used by Mhaiskar and Mandal (1996) and Zhang et al. (2010a, b), as described later.

To reach an equivalent single layer, first, the upper "$n-1$" layers of thicknesses $H_1, H_2, H_3, \ldots$ and H_{n-1} (Fig. 4.17) should be replaced by a single layer of thickness ($H_{\text{eff}} = H_1 + H_2 + H_3 + \cdots + H_{n-1}$) having an equivalent modulus of E_H in Fig. 4.18a
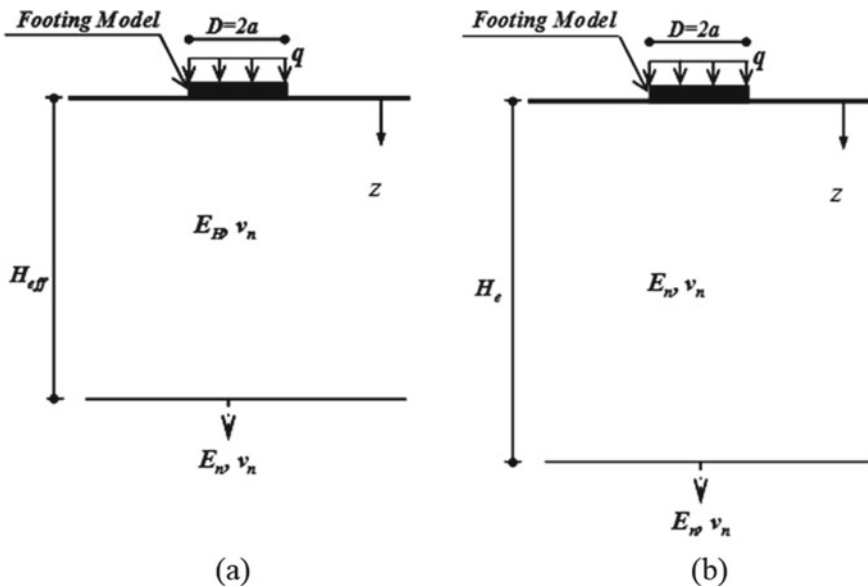
Fig. 4.18 Substituting n-layer system sequentially with **a** Equivalent two-layered system for n-layer system in Fig. 4.17, **b** equivalent single-layer system with the same E_n and v_n for two-layered system in Fig. 4.18a

(Hirai 2008). The equivalent elastic modulus (E_H) of layers 1 to $n - 1$, is calculated by using Eq. (4.17) for the footing with no embedment depth ($D_f = 0$) as Eq. (4.28).

$$E_H = \left[\sum_{j=1}^{n-1} \left\{ E_i \frac{(1 - v_n^2)}{\left(1 - v_j^2\right)} \right\}^{\frac{1}{3}} \frac{H_j}{H_{\text{eff.}}} \right]^3 \tag{4.28}$$

where, H_i and E_i are the thickness and elastic modulus of ith layer, respectively. The n-layer system in Fig. 4.17 is thus reduced to a two layers system as shown in Fig. 4.18a.

The two-layered system (Fig. 4.18a) can be reduced to an equivalent single-layer system (Fig. 4.18b) with elastic modulus of E_n and an equivalent thickness of H_e. The equivalent thickness (H_e) with the elastic modulus of E_n and Poisson's ratio of v_n is then defined by Eq. (4.29) for the case where $E_H \geq E_n$ and by Eq. (4.30) for the case where $E_H \leq E_n$. Equations (4.29) and (4.30) provided for the same Poisson's ratio of the two layers in Fig. 4.18a where E_n is the elastic modulus of the nth layer.

$$H_e = \left(\frac{E_H}{E_n} \right)^{1/3} H_{eff} \tag{4.29}$$

$$H_e = \left[0.75 + 0.25 \left(\frac{E_H}{E_n} \right)^{1/3} \right] H_{eff} \tag{4.30}$$

Consequently, the use of Eqs. (4.28)–(4.30) deliver an equivalent single homogeneous semi-infinite mass of material that can be substituted for the n-layer system as shown in Fig. 4.18b. Generally, the footing settlement (i.e., soil surface settlement), w should be calculated using Eqs. (4.24)–(4.27). Since the nature of footing pressure-settlement variation is nonlinear, the behavior of unreinforced layers and reinforced layers (Geocell and soil inside of its pockets) are considered to act as MLE (Multiple Linear Elastic) layers. The MLE model provides an ability to calculate the elastic modulus of each layer, for each load step, using the confining pressure of the current and previous stages as described in Eqs. (4.31)–(4.42).

To calculate the elastic modulus of the ith layer requires knowledge of the strain of layers 1 to $n - 1$. To compute these, the deformation and equivalent thickness of the ith layer (Fig. 4.17) are required. Using Eqs. (4.20)–(4.23) for the footing with no embedment depth ($D_f = 0$), supported on a multi-layer system, the equivalent thickness of each soil layer, H_{ie} with the same E_n and v_n was determined by Eq. (4.31) for the case where $E_i \geq E_n$ and by Eq. (4.32) for the case where $E_i \leq E_n$, respectively.

$$H_{ie} = \left\{ \frac{E_i \left(1 - v_n^2\right)}{E_n \left(1 - v_i^2\right)} \right\}^{1/3} H_i \tag{4.31}$$

$$H_{ie} = \left[0.75 + 0.25 \left\{ \frac{E_i \left(1 - v_n^2\right)}{E_n \left(1 - v_i^2\right)} \right\}^{1/3} \right] H_i \tag{4.32}$$

Then, from Eqs. (4.24) and (4.26), for a rigid circular footing with radius "a" subjected to uniform pressure "q", the thinning and strain of the ith layer are defined as Eqs. (4.33)–(4.35).

$$w_i = \frac{2\pi a q \left(1 - v_n^2\right)}{4E_n} \left(\sqrt{1 + \left(\frac{\sum_{l=1}^{l=i} H_{le}}{a} \right)^2} - \frac{\sum_{l=1}^{l=i} H_{le}}{a} \right)$$

$$\left(1 + \frac{\sum_{l=1}^{l=i} H_{le}}{2a(1 - v_n)\sqrt{1 + \left(\frac{\sum_{l=1}^{l=i} H_{le}}{a} \right)^2}} \right) \tag{4.33}$$

$$w_{p_i} = \frac{E_n}{E_i}(w_i - w_{i-1}) \tag{4.34}$$

$$\varepsilon_i = \frac{w_{p_i}}{H_i} \tag{4.35}$$

where

H_{ie} equivalent thickness of the ith layer based on the elastic parameters of the nth layer

w_i displacement at a depth of $\sum_{l=1}^{l=i} H_{le}$

w_{pi} the vertical deformation within the ith layer of thickness H_{ie}, (due to actual thinning of the ith layer)

ε_i the strain across the thickness of the ith layer.

In the jth loading step, the displacement increment of soil surface due to loading increment of $q_j - q_{j-1}$ can be calculated by Eqs. (4.36)–(4.39).

$$\Delta w_1^j = \frac{2\pi a (q_j - q_{j-1})\left(1 - v_n^2\right)}{4E_n} \left(\sqrt{1 + \left(\frac{H_e}{a} \right)^2} - \frac{H_e}{a} \right)$$

$$\left(1 + \frac{H_e}{2a(1 - v_n)\sqrt{1 + \left(\frac{H_e}{a} \right)^2}} \right) \tag{4.36}$$

$$\Delta w_0^j = \frac{2\pi a \left(1 - v_n^2\right)(q_j - q_{j-1})}{4E_n} \tag{4.37}$$

$$\Delta w_2^j = \frac{E_n}{E_H} \left(\Delta w_0^j - \Delta w_1^j \right) \tag{4.38}$$

$$w^j = w^{j-1} + \Delta w_1^j + \Delta w_2^j \tag{4.39}$$

where:

Δw_1^j vertical displacement increment on loading centerline at a depth of H_e for loading increment of $q_j - q_{j-1}$, (i.e. at the bottom of the equivalenced layer),

Δw_0^j vertical displacement increment at surface (of equivalent layer) beneath centre of load for loading increment of $q_j - q_{j-1}$,

Δw_2^j vertical deformation (thinning) increment of the original layer of thickness of H,

w^j vertical displacement at surface of the system for loading of q_j.

Similarly, the strain increment for the ith layer at the jth loading step can be calculated using Eqs. (4.40)–(4.42) using the adjustments already employed to formulate Eqs. (4.14) and (4.16).

$$\Delta w_i^j = \frac{2\pi a(q_j - q_{j-1})(1 - \upsilon_n^2)}{4E_n}\left(\sqrt{1 + \left(\frac{\sum_{l=1}^{l=i} H_{le}}{a}\right)^2} - \frac{\sum_{l=1}^{l=i} H_{le}}{a}\right)$$

$$\left(1 + \frac{\sum_{l=1}^{l=i} H_{le}}{2a(1 - \upsilon_n)\sqrt{1 + \left(\frac{\sum_{l=1}^{l=i} H_{le}}{a}\right)^2}}\right) \tag{4.40}$$

$$(\Delta w_p)_i^j = \frac{E_n}{E_i}\left(\Delta w_i^j - \Delta w_{i-1}^j\right) \tag{4.41}$$

$$\varepsilon_i^j = \varepsilon_i^{j-1} + \frac{(\Delta w_p)_i^j}{H_i} \tag{4.42}$$

where:

H_{ie} equivalent thickness of the ith layer based on the elastic parameters and thickness of the nth layer as defined by Eqs. (4.31 and 4.32),

Δw_i^j displacement increment of equivalent layer for layers 1 to i based on the elastic parameters of nth layer in depth of $\sum_{l=1}^{l=i} H_{le}$ for loading increment of $q_j - q_{j-1}$,

$(\Delta w_p)_i^j$ deformation increment (thinning) of layer with thickness of H_i for loading increment $q_j - q_{j-1}$,

ε_i^j strain of layer with thickness of H_i subjected to loading q_j.

4.3.2.1 Results and Discussion

As can be seen, one of the contributing factors in settlement equations is elastic modulus of both geocell-reinforced and unreinforced soil layers. Since one of the
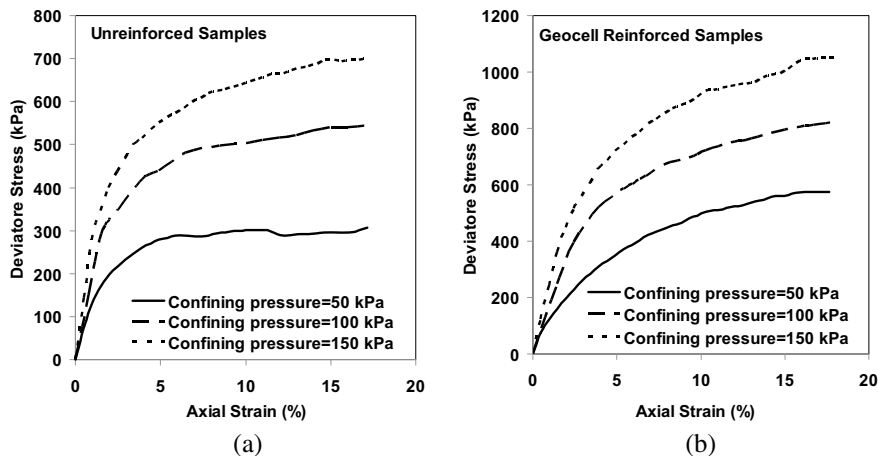
Fig. 4.19 Stress-axial strain curves for unreinforced and geocell-reinforced samples under confining pressure of 50, 100 and 150 kPa **a** unreinforced samples, **b** geocell-reinforced samples (Noori 2012)

most useful tests in determination of soils' elastic modulus is triaxial compression tests, herein the process of obtaining the elastic modulus of unreinforced and geocell-reinforced soil layers in terms of strain and confining pressure, $E = f(\sigma_3, \varepsilon)$ for each loading step, is presented.

(a) *Elastic modulus of unreinforced layers*

Based on the data extracted from Fig. 4.19a, the vertical stress ($\sigma_1 = \sigma_3 + \sigma_d$) of triaxial samples was found to be a function of the confining pressure (σ_3) and axial strain (ε). Therefore, according to Eq. (4.43) a nonlinear regression model was developed to estimate the vertical stress (σ_1) for different values of σ_3 and ε.

$$\sigma_1 = 61.47 \, \sigma_3^{0.73} \, \varepsilon^{0.34} \, e^{-3.17\varepsilon} \tag{4.43}$$

The tangential modulus of elasticity can be derived as the derivative of stress with respect to strain (from Eq. 4.43) as presented in Eq. (4.44). The function of $f(\varepsilon)$ is defined in Eq. (4.45).

$$E = 61.47 \, \sigma_3^{0.73} * f(\varepsilon) \tag{4.44}$$

$$f(\varepsilon) = \left(-3.17 \, e^{-3.17\varepsilon} \varepsilon^{0.34} + \frac{0.34 \, \varepsilon^{0.34}}{\varepsilon} e^{-3.17\varepsilon} \right) \tag{4.45}$$

(b) *Elastic modulus of geocell-reinforced layers*

Madhavi Latha (2000), based on the results of triaxial compression tests on geocell-encased sand, proposed an empirical equation in the form of Eq. (4.46) to express

the elastic modulus of the geocell-reinforced sand (E_g).

$$E_g = 4\,\sigma_3^{0.7}(K_u + 200M^{0.16})$$ (4.46)

where

K_u the dimensionless modulus number of the unreinforced sand in the hyperbolic
model proposed by Duncan and Chang (1970),

M the secant tensile modulus of the geocell material (e.g., geotextile and geogrid)
in *kN/m,* assessed at an average strain of 2.5% in load-elongation, and

σ_3 the confining pressure in kPa.

In fact, the geocell layers are modeled as equivalent composite layers with enhanced stiffness and shear strength properties. The term in parentheses of Eq. (4.46) expresses Young's modulus parameter of geocell-reinforced soil in terms of the secant modulus of the geocell material (M) and the dimensionless modulus number of the unreinforced soil (K_u).

However, due to the fact that the suggested relationship by Madhavi Latha (2000), Eq. (4.46), is not a function of axial strain level, it is modified to Eq. (4.47) as a function of both confining pressure (σ_3) and axial strain (ε).

$$E_g = a_1\,\sigma_3^{b_1}\,(K_u + a_2 M^{b_2}) * f(\varepsilon)$$ (4.47)

The function of $f(\varepsilon)$ is assumed as Eq. (4.45) and then the parameters of a_1, a_2, b_1, and b_2 are obtained from the triaxial test results of geocell-reinforced soil (Fig. 4.19b). The constants parameters in Eq. (4.47) depend on the type of infill soil and strength of geocell material, which must be calibrated according to the results of triaxial tests on soil and geocell, with the same properties that would be used in the foundation bed. Fitting Eq. (4.47) to the data of Noori (2012) yields the elastic modulus as a function of σ_3, ε, K_u and M as Eq. (4.48).

$$E_g = 0.12\,\sigma_3^{0.73}\,(K_u + 100M^{0.1}) * f(\varepsilon)$$ (4.48)

At each loading step, the elastic modulus of unreinforced and reinforced layers was estimated using the confining pressure (at mid-height of the layer) and the strain computed at the end of the previous loading step. The confining pressure in the middle of each reinforced layer was obtained by multiplying the distributed vertical stress by the coefficient of lateral pressure (k_r) calculated in Eq. (4.49). The value of lateral pressure coefficient for unreinforced soil $k_{un} = 0.5$ has been suggested by Madhavi Latha (2000). For $M = 0$, Eq. (4.49) results in the lateral pressure coefficient of unreinforced soil (k_{un}).

$$k_r = k_{un}\,(K_u + 100M^{0.1})/K_u$$ (4.49)

Overall, Eqs. (4.44)–(4.49) reveal that the proposed formulations would be able to consider the variation of geocell performance in regard to the strain level and confinement stress variations across the depth of the foundation bed, provided the elastic modulus of the different layers (soil layers and the geocell-reinforced layers) are allotted appropriate values that differ from layer-to-layer and from one loading step to the next. Based on the results of triaxial compression tests, the value of the hyperbolic parameter of Duncan and Chang (1970), K_u, is found as 483.3 (the authors' evaluation not reported here). Also, the secant modulus of the geocell material at 2.5% strain, M, is given by the manufacturer as 114 kN/m ($M = 114$ kN/m). Due to the confinement of the soil by the geocell wall, the Poisson's ratio of geocell-reinforced layers may be less than that in unreinforced layers. The range of Poisson's ratio for granular soil (i.e. sand in the present paper) is about 0.3–0.35 and for geocell filled with sand from 0.17 (Mhaiskar and Mandal 1996) to 0.25 (Zhang et al., 2010a, b). Thus, a Poisson's ratio of 0.3 is used for unreinforced layers, and a Poisson's ratio of 0.25, 0.2, and 0.2, is used, respectively for reinforced layers with one, two, and three layers of geocell.

4.3.2.2 Validation of Proposed Analytical Method

The presented analytical method was validated by comparing the results of model analyses with plate load test results (Moghaddas Tafreshi et al. 2013) for an unreinforced bed and for beds reinforced by three layers of geocell. Figure 4.20 compares the results of the analytical method and tests in the form of footing pressure-settlement responses, for different values of geocell mass. These comparisons are done for parameters of $K_u = 483.3$, $M = 114$ kN/m, $h_g = 100$ mm and $D = 300$ mm. Since
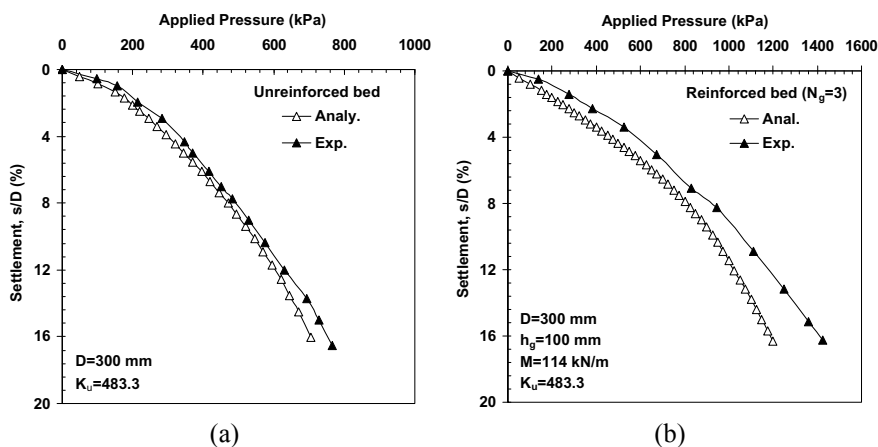

Fig. 4.20 Comparison of analytical and experimental results for **a** unreinforced bed, **b** reinforced bed with three layers of geocell (Moghaddas Tafreshi et al. 2015)

the analytical method has not considered any variation in the geocells' width; it is assumed that the width of the geocell-reinforced layers being sufficient to ensure the anchorage derived from the adjacent stable soil mass.

The predicted responses show a better match with the experimental ones at lower footing settlement levels (i.e., $s/D < 8\%$). For larger footing settlements (e.g., $s/D > 8\%$), the analytical predictions underestimate the experimentally determined settlements, implying strain softening in the geocell-soil layers in situ relative to the performance in the triaxial or that the assumption of no lateral strain is non-conservative. The difference between the predicted responses and experimental ones might more generally be attributed to the selected value of lateral pressure coefficient, the selected values of Poisson's ratio, the simplifying assumptions used in the analytical method, the discrepancies between the experimental and analytical systems and the differences in simulating the field and the experimental conditions of multiple layers.

Since the practical design of shallow footings is mostly governed by footing settlement, footing settlement must be limited to specific values, depending on the super-structure. Thus, the close comparison of analytical and experimental results in the lower range of settlement (i.e., less than 6% of the footing diameter) is encouraging. This implies that the analytical method presented is capable of estimating the behavior of footings supported by geocell layers and maybe conveniently applied as a tool to estimate the pressure-settlement response of footings over most practical ranges of geotechnical use.

4.4 Contributing Factors

Moghaddas Tafreshi et al. (2015) carried out a parametric study using the analytical model presented to understand how the considered parameters affect the response of the geocell-reinforced foundations. The investigated parameters comprised variation in the secant modulus of geocell (M), the dimensionless modulus number of the soil (K_u), the thickness of geocell layers (h_g), and the number of geocell layers (N_g).

Figure 4.21a shows the effect of the secant modulus of the geocell (M) on the pressure-settlement response of a foundation reinforced with three layers of geocell. The results reveal the beneficial effect of the reinforcement's rigidity (see Eq. 4.48) in decreasing the footing settlements so that at a given bearing pressure, the value of the settlement decreases as the secant modulus of geocell (M) increases. The similar results reported by Madhavi Latha et al. (2006) for geocell-supported embankments showed that higher surcharge capacity and lower deformations are associated with an increase in the value of the M parameter. This performance could be attributed to the internal confinement provided by geocell reinforcement with an increase in M. The confinement effect is dependent on the secant modulus of the reinforcement, the friction at the soil-reinforcement interface and the confining stress developed on the infilling soil inside the geocell pocket due to the passive resistance provided by the 3D structure of geocell (Sireesh et al. 2009; Moghaddas Tafreshi and Dawson
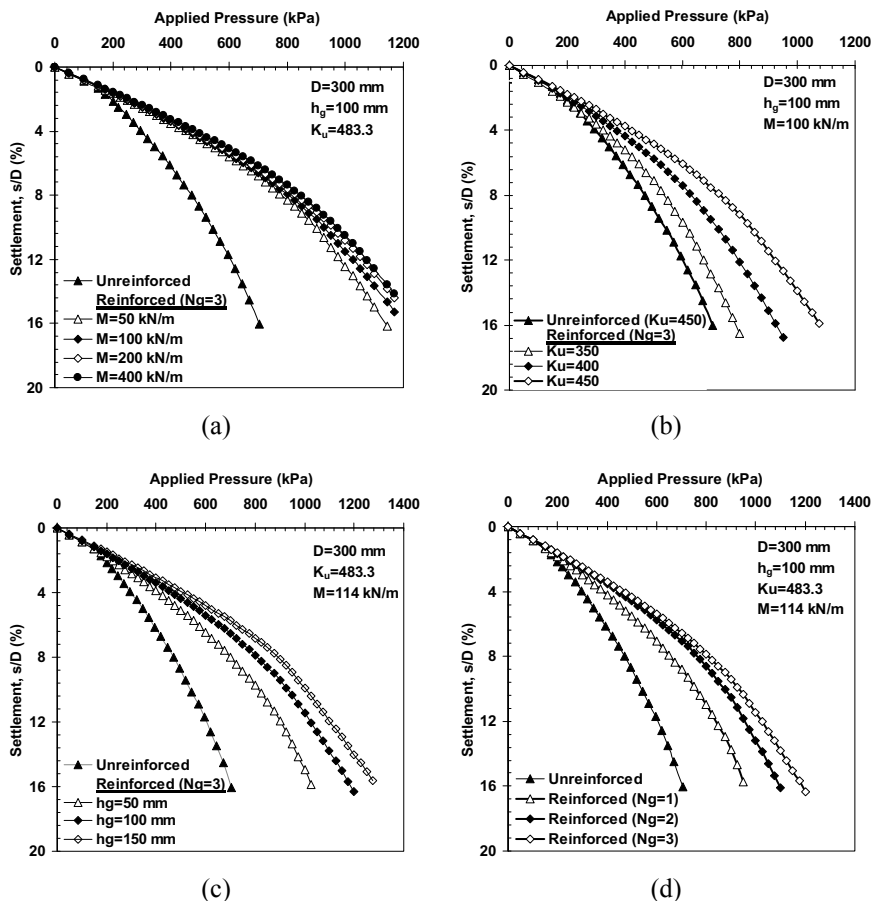
Fig. 4.21 Variation of pressure-settlement response of geocell-reinforced bed for different **a** secant modulus of geocell (M), **b** soil dimensionless modulus (K_u), **c** thickness of geocell layers (h_g), and **d** number of geocell layers (N_g) (Moghaddas Tafreshi et al. 2015)

2010a). In addition, as seen in Fig. 4.21a, there is a limiting value of M (=100 kN/m) beyond which no further load-settlement benefit is achieved. Almost certainly this is because the behavior of the unreinforced soil between the reinforced layers is now limiting the response of the overall system.

To see what the effect of K_u is, the variation of pressure-settlement of the reinforced bed with three layers of geocell is presented in Fig. 4.21b. The results show that the bearing capacity of a footing at a given settlement is significantly increased due to an increase in the K_u value. Thus, the role of the soil type and the soil compaction in the performance of geocell-reinforced beds, which the composite model suggested in the present study, can take into account this effect. However, a dense sand matrix tends to dilate under footing penetration, thereby mobilizing higher strength in the

geocell reinforcement, leading to greater performance improvement (Madhavi Latha et al. 2009).

The rigidity of the geocell layer is predominantly influenced by the thickness of geocell. To have a better assessment of the effect of a geocell's thickness in a geocell-reinforced foundation, the variation of the pressure-settlement relationship of the unreinforced bed and of the reinforced bed with three layers of geocell is presented in Fig. 4.21c. The benefit of a thicker geocell mat is evident, so that a thicker geocell decreases the footing settlements, tending to improve its bearing capacity. This appears to be a consequence of greater opportunity of geocell-soil interaction (in the form of wall-friction and confining pressure imposed by the pocket walls) and the increased stiffness of the effective zone beneath the footing consequent upon an increase in the thickness of geocell. This is in line with the findings of Dash et al. (2007), Madhavi Latha et al. (2006) Moghaddas Tafreshi and Dawson (2010a) who reported that the settlement of a trench's soil surface was decreased due to the provision of a thicker geocell in the backfill. Furthermore, the rate of reduction in footing settlement and the rate of enhancement in load-carrying capacity of the footing can also be seen to reduce with an increase in the value of h_g. The reason is that, as multiple, thicker reinforcement layers are used, then the reinforced zone extends deeper beyond the zone most significantly strained by the applied load, so that little further benefit accrues. From a practical point of view, as the thickness of a geocell layer is increased; the problem of lower achieved compaction in the geocell packets would be encountered, so that higher compactive effort is necessary as the thickness of vertical webs of the geocell is increased, owing to hindering of vertical densification (Thakur et al. 2012; Tavakoli Mehrjardi et al. 2013). For this reason, multiple thin geocell layers may, in practice, be preferred to fewer, thicker layers.

Figure 4.21d presents the bearing pressure-settlement response of the unreinforced and reinforced foundation beds with one, two, three layers of geocell. From this figure, it may be clearly observed that, as the number of geocell layers increases (i.e., the increase in the depth of the reinforced zone), both stiffness and bearing pressure at a specified settlement increase substantially. Likewise, at a given bearing pressure, the value of the settlement decreases as the number of geocell layers increases. However, the rate of reduction in footing settlement is seen to reduce with an increase in the number of geocell layers. It is likely that the additional layers are interacting with soil that is strained less and less by the applied load, therefore delivering diminishing increments of additional reinforcement effect. Yoon et al. (2008) and Moghaddas Tafreshi et al. (2013) in their studies on the effect of multi-layered geocell reported a similar effect with increase in the number of 3D reinforcement layers.

The reinforcing effects of multiple layers of geocell in sand were also measured using plate loading at a diameter of 300 mm (Moghaddas Tafreshi et al. 2013). Granular soil passing through the 38 mm sieve with a specific gravity of 2.68 (G_s = 2.68) was used as backfill soil in the testing program which is classified as well-graded sand. The maximum dry density was about 20.62 kN/m^3, which corresponds to an optimum moisture content of 5.7%. The average measured dry densities of unreinforced soil and the soil filled in geocell pockets after compaction of each layer were 18.56 and 18.25 kN/m^3. Figure 4.22a presents the bearing pressure-settlement
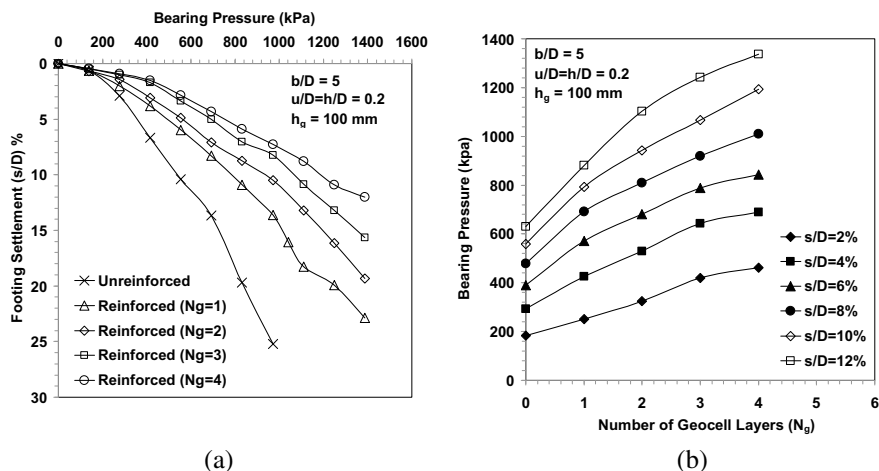
Fig. 4.22 Variation of bearing pressure with **a** the footing settlement for the unreinforced and geocell-reinforced foundation beds with one, two, three, and four layers of geocell, and **b** the number of geocell layers at different levels of settlement (Moghaddas Tafreshi et al. 2013)

behavior of the unreinforced and reinforced foundation beds with one, two, three and four layers of geocell ($N = 1, 2, 3, 4$) when the layers of geocell were placed at the optimum values of u/D and h/D ($u/D = h/D = 0.2$).

From Fig. 4.22, it may be clearly observed that as the number of geocell layers increased (i.e. with the increase in the depth of the reinforced zone), both stiffness and bearing pressure at a specified settlement increase substantially. This figure shows that no clear bearing capacity failure point was evident, even at a settlement level of 20–25%, regardless of the mass of geocell in the foundation bed. Beyond a certain footing settlement level—that is, at s/D around 2–4%, depending on the mass of reinforcement beneath the footing base—there was an increase in the slope of the settlement–pressure curves. This may be attributed to local foundation breakage in the region under and around the footing, because of high deformation induced by the large settlement under the footing. This would lead to a reduction in the load-carrying capacity of the footing as indicated by the softening in the slope of the pressure-settlement responses. Beyond this stage, the slope of the curves remained almost constant with the footing bearing pressure continuously increasing, suggesting that this mode of damage developed progressively. In order to have a direct comparison of the results for the unreinforced and multi-layered geocell-reinforced beds, the bearing pressure values corresponding to settlement ratios of 2, 4, 6, 8, 10, and 12% were extracted from Fig. 4.23a for different numbers of geocell layers. Figure 4.22b plots these data against the number of geocell layers (N_g). This range of settlement levels (less than 12%) was selected to reflect a range of practical interest. It can be seen that as the number of geocell layers increased, the bearing pressure increased steadily, regardless of the settlement ratio. For example, at the settlement ratio of $s/B = 4\%$, the bearing capacity values were about 292, 427, 530, 642, and 688 kPa
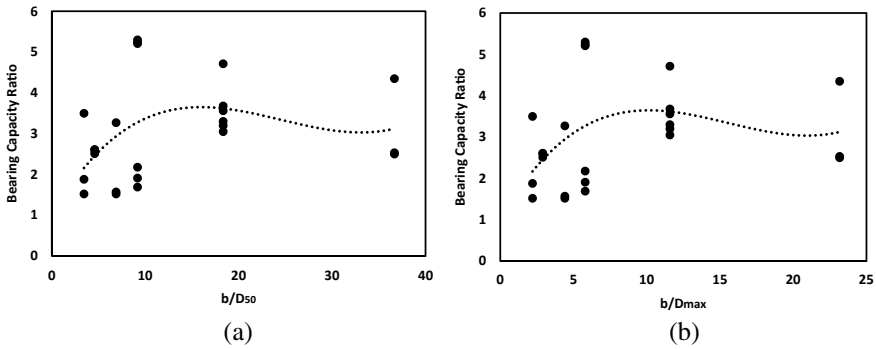
Fig. 4.23 Variation of bearing capacity ratio versus the ratio of the geocell's cells size to **a** the medium grains size (D_{50}), **b** the maximum grains size (D_{max}) (Tavakoli Mehrjardi et al. 2019)

for unreinforced bed, and reinforced bed with one, two, three and four layers of geocell, respectively. Thus the increases in bearing pressure were about 46, 82, 120, and 135% for one, two, three, and four layers of geocell reinforcement, respectively. A comparison with Fig. 4.22a shows that this increased bearing pressure was a consequence of the increased stiffness consequent upon geocell reinforcement. At low settlement ratios, $s/D < 4\%$, the benefit of three reinforcing layers is evidenced by the higher gradient of the lines in the figure. For practical applications, small settlements are almost always needed and three reinforcing layers are associated with the greatest bearing pressure increase for the same settlement.

Fig. 4.22b also indicates that the benefits of reinforcement increase as the footing settlement increases. This performance could be attributed to the internal confinement provided by geocell reinforcement. The concept of confinement reinforcement, which may be called internal confinement, was explained by Yang (1974). The confinement effect is dependent on the tensile strength of the reinforcement, the friction at the soil-reinforcement interface and the confining stress developed on the infilling soil inside the geocell pocket due to the passive resistance provided by the 3D structure of geocell (Sitharam and Sireesh 2005). Obviously, the reinforced system must exhibit some settlement, and consequently, strain (elongation) must develop in the reinforcement layers to affect the geocell modulus, tensile and frictional strength, and the passive resistance offered by the geocell layers. Additionally, this comparison indicates that it is necessary to consider the footing settlement level while investigating the effects of reinforcement on the bearing pressure of reinforced sand.

Among the effective parameters on the performance of geocell-reinforced foundations, the situation of geoccell embedment and also, the width of geocell layers expanded beneath the footings have been discussed by previous researchers. Table 4.3 presents the optimum values for the burial depth of the first geocell layer (u), the vertical spacing of geocell layers, in multi-layered systems, (h) and width of geocell (b).

Table 4.2 Relationships for bearing capacity of geocell-reinforced foundations

Researcher	Mechanism considered	Bearing capacity equation	Parameters
Koerner (1998)	Lateral resistance effect	$p_r = 2p\tan^2(45 - \emptyset/2)\tan\delta + cN_cS_c + qN_qS_q + 0.5\gamma BN_\gamma S_\gamma$	p = applied pressure on geocell matress (kPa) $\emptyset$ = friction angle of the soil used to fill the geocell pocket (degrees) c = cohesion of the soil (kPa) q = surcharge load (kPa) γ = unit weight of the soil (kN/m³) N_c, N_q, N_γ = bearing capacity factors S_c, S_q, S_γ = shape factors
Presto (2008)	N/A	$p_r = 2\frac{h}{d}k_a\sigma_{vm}\tan\delta + c_uN_c$	k_a = coefficient of active earth pressure σ_{vm} = average vertical stress (kPa) c_u = subgrade shear strength (kPa) N_c = bearing capacity coefficient
Avesani Neto et al. (2013)	Confinement effect, stress dispersion effect and the membrane effect	$p_r = p_u + 4\frac{h}{d}k_0pe\tan\delta + (1 - e)p$	e = stress redistribution effect
Sitharam and Hegde (2013)	Lteral resistance effect, vertical stress dispersion and membrane mechanisms	$p_r = p_u + 2p\tan^2(45 - \emptyset/2)\tan\delta +$ $p_r\left(1 - \frac{B}{B+2D_r\tan\beta}\right) + \frac{4TS}{B_gB}$	$\emptyset$ = friction angle of the soil used to fill the geocell pockets (degrees) D_r = depth of the reinforcement (m) βn = load dispersion angle (degrees) T = tensile strength of the basal geogrid material (kN/m) B_g = width of the basal geogrid (m) S = footing settlement measured at the surface (m)

It should not lose sight of the fact that the beneficial performance of geocell is absolutely dependent on its installation in the backfill. Tavakoli Mehrjardi et al. (2013) observed the importance of compaction both below and above the level of the geocell installation. On the other hand, if the geocell is situated on low-density backfill layer, it gives rise to poorer performance of the geocell even compared with the unreinforced status. In effect, the vertical webs of the geocell hindered vertical densification. Necessarily, they must also stop inter-meshing of stones in adjacent pockets of the web structure. Consequently, the effective reinforcement and improvement of the backfill system are achievable if the geocell is installed in the backfill with an appropriate compaction process.

4.5 Scale Effects

Performance of a system in the context of physical modeling is directly dependent on geometrical matters and considered aspect ratio. In other words, a study about the scale effect is absolutely timely and crucial in the interpretation of the obtained results, especially when it applies to prototype and practical models. Many experimental studies in the field of reinforced embankments have been carried out with small or large-scale physical modeling at which the scale effects are rarely fully considered. However, one of the most challengeable matters in this area is how the reduced-scale model and prototype model tests can be bridged. Recently, some experimental and numerical studies have been carried out to understand the parametric sensitivity of geogrid-reinforced soil (Góngora and Palmeira 2016; Brown et al. 2007; Cuelho et al. 2014; Tavakoli Mehrjardi and Khazaei 2017; McDowell et al. 2006). Table 4.4 summarizes the optimum values for a different studied parameter. In this table, "a_{eq}" is equal aperture size of geogrids; "B" is loading plate's diameter; "D_{50}" is the medium aggregates size, and "D_{max}" is maximum aggregates size.

Although many investigations have been carried out on geogrid-soil interactions, there is a serious lack of studies on the response of geocells in soil medium with regard to the geometrical variations. Tavakoli Mehrjardi et al. (2019) carried out a series

Table 4.3 The optimum values for the burial depth of first geocell layer (u), the vertical spacing of geocell layers, in multi-layered systems, (h) and width of geocell (b)

Researcher	u	h	b
Sireesh et al. (2009)	NE[a]	NE[b]	4.9D
Dash et al. (2001)	0.1B	NE[b]	4B
Sitharam and Sireesh (2005)	0.05B	NE[b]	5B
Moghaddas Tafreshi and Dawson (2010a)	0.1B	NE[b]	3.2B
Moghaddas Tafreshi et al. (2013)	0.2B	0.2B	NE[a]

[a]*NE* Not evaluated
[b]*NE* Not evaluated due to use the single geocell layer

Table 4.4 The optimum values for proposed aspect ratio in geogrid-reinforced foundations

Researchers	a_{eq}/D_{50}	a_{eq}/D_{max}	B/D_{50}	a_{eq}/B
McDowell et al. (2006)	NE[a]	1.4	NE	NE
Brown et al. (2007)	NE	1.2–1.6	NE	NE
Cuelho et al. (2014)[b]	3.9	1.2	NE	NE
Góngora and Palmeira (2016)	NE	0.7–1.35	NE	NE
Tavakoli Mehrjardi and Khazaei (2017)	4	2.1–2.6	13–25	0.2

[a]*NE* not investigated
[b]referred by Palmeira and Góngora (2016)

of plate load tests to investigate the sensitivity of reduced-scale geocell-reinforced soil to variation of deciding key factors, notably loading plate size, soil grain size, and geocell's opening size. Four types of uniformly graded soils as backfill materials with the medium grain size (D_{50}) of 3, 6, 12, and 16 mm were considered. The utilized geocells made of heat-bonded nonwoven geotextile had the cell equivalent diameter/height of 55/50 and 110/50 mm, respectively (Table 4.4).

The major physical parameters influencing the response of geocell-reinforced backfill systems can be summarized as B, u, L, D_{50}, γ, E_{soil}, E_{GC}, and b; where "γ" and "E_{soil}" are unit weight and secant elastic modulus of the backfill, respectively, "E_{GC}" is the elastic modulus of geocells, "u" is the burial depth of geocell, "B" is loading plate's diameter, and "L" is the width of geocells expanded beneath the loading plate. The function (f) that governs the geocell-reinforced backfill systems can be written as Eq. (4.50).

$$q_u = f(B, u, L, D_{50}, \gamma, E_{soil}, E_{GC}, b) \tag{4.50}$$

The equation comprises eight parameters containing two fundamental dimensions (i.e., length and force). Therefore, Eq. (4.50) can be reduced to six independent parameters (π_1, π_2, π_3, …, π_6) and substituted with Eq. (4.51). As can be seen, the obtained non-dimensional parameters could predominantly affect the response of geocell-reinforced systems. The similarity in response is achievable if the π terms, both for model and prototype are equal.

$$\frac{q_u}{\gamma B} = f\left(\frac{u}{B}, \frac{h}{B}, \frac{D_{50}}{B}, \frac{\gamma D_{50}}{E_{soil}}, \frac{E_{soil}}{E_{GC}}, \frac{b}{D_{50}}\right) \tag{4.51}$$

As an example, assuming that the soils used in the model and prototype do have the same unit weight and footing diameter of a prototype model (B_p) is n times as many as that of the test model (B_m), Eq. (4.52) can be satisfied to obtain the bearing capacity of prototype system.

$$\left(\frac{q_u}{\gamma B}\right)_m = \left(\frac{q_u}{\gamma B}\right)_p \xrightarrow{\text{yields}} (q_u)_p = n(q_u)_m \tag{4.52}$$

Herein, some questions have arisen in this study: what is the effect of aggregates size? What is enough loading plate size to minimize the scale effect? Is there any optimum cells size for a geocell to provide maximum reinforcement efficiency?

One of the major issues in approaching the optimal design of geocell-reinforced backfill is to understand the fundamental mechanics of aggregate/geocell interactions. In particular, it should be possible to optimize the mechanical and geometric properties of the geocell, gaining maximum reinforcement efficiency. In this respect, according to Fig. 4.23a, studying the variation of bearing capacity ratio versus the ratio of the geocell's cells size (b) to the medium grains size (D_{50}) can be predominant. It is clearly seen that the highest values of BCR, irrespective of the loading plate size, are attainable when the ratio b/D_{50} is in the range of 12–18. Reasonably, it is certified that the optimum nominal cell size of geocells is about 15 times of medium grain size of soil. In other words, in the case of larger backfill's particles (left side of the mentioned range), geocell/backfill interactions get deteriorated, resulted in reduction in bearing capacity ratio. On the other side, for the smaller backfill's particles or larger geocell's cells ($b/D_{50} > 15$), less stone–stone interactions are provided and therefore, lateral buckling of particles columns in the geocell's plane is encountered and eventually, bearing capacity ratio is reduced, dramatically. Much as there is no available data on the effectiveness of b/D_{50} for geocell-reinforced system, Tavakoli Mehrjardi and Khazaei (2017) and Cuelho et al. (2014), reported that restricting the ratio of the geogrid's apertures size to the medium grains size to the value of about 4, had the highest beneficial circumstances on geogrid-reinforced backfill behavior. Also, Tavakoli Mehrjardi et al. (2016), by conducting plate load tests on poor-graded fine and coarse sands and reinforced by geogrids, found out that the ratio of the geogrid apertures sizes to the medium soil grains sizes is a deciding factor in the interaction between soil's grains and geogrid.

Moreover, to see variations of bearing capacity ratio versus the ratio of the geocell's cells size to the maximum grains size (b/D_{max}), Fig. 4.23b is illustrated. Accordingly, there is an optimum range of 7–11 for (b/D_{max}) ratio which affords the maximum bearing capacity ratio.

Although practically, footing width is much greater than soil's medium grains size, in geotechnical test methods (plate load test; in particular), special attention should be given to the ratio of the loading plate size (B) to the medium grains size (D_{50}). With this respect, Fig. 4.24 presents the variation of bearing capacity ratio versus the ratio of the loading plate size to the medium grains size (B/D_{50}). According to the observed variations, the best efficiency of geocell reinforcement has been achieved for the optimal amount of B/D_{50} in the range of 13–27 (approximately 20; in average). In the outer of the mentioned optimum range, BCR decreased drastically. In the line with this conclusion, Tavakoli Mehrjardi and Khazaei (2017) observed that in order to obtain the highest benefits from geogrid reinforcement in geogrid-reinforced backfill, the footing's width should be in the range of 13–25 times of medium grain size. Moreover, Hsieh and Mao (2005) reported when the loading plate's diameter was larger than 15 times the D_{50} of the soil test, no marked influence of plate size on surface settlement would be expected.

Fig. 4.24 Variation of bearing capacity ratio versus the ratio of the loading plate's diameter (B) to the medium grains size (D_{50}) (Tavakoli Mehrjardi et al. 2019)
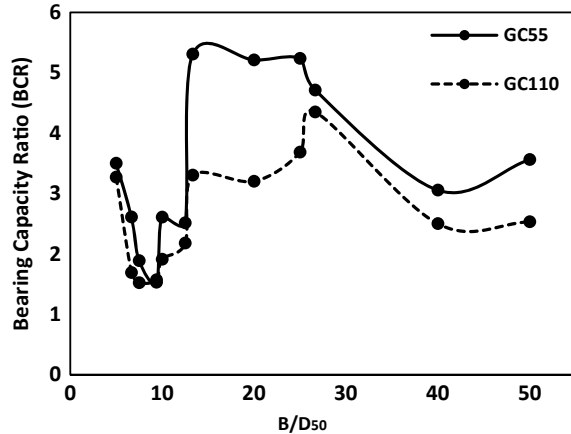
According to Eq. (4.50) and based on dimensional analysis rules (see Eq. 4.51), the studied length-dimensional parameters including B, $D_{50,}$ and b can at most be converted to two independent non-dimensional parameters. Previously, the importance of non-dimensional parameters, namely B/D_{50} and b/D_{50} was explained. This means that the r*atio of the loading plate size to the geocell cells sizes (B/b)* does not seem to be a contributory parameter in the bearing capacity ratio. This is the exact reason for placement of B/D_{50} and b/D_{50} as independent parameters in Eq. (4.51). From this point of view, by taking right precautions, it can be concluded that the B/b ratio should be selected larger than 1.5 which could provide a more stable and reliable geocell-reinforced backfill. This statement is more likely to be useful if the surface stress would be applied over a small area such as tire print, railway sleeper, or footprint. In fact, geocells possessing large cells in comparison with footing size (small values of B/b) ruin the beneficial role of reinforcement in that each cell does likely behave as an unreinforced soil element (Tavakoli Mehrjardi et al. 2019).

4.6 Comparing the Performances of Geocell and Planar Reinforcements

Geocell is an advantageous soil-reinforcement method that can provide stiffer and stronger foundations compared to planar reinforcement methods. Due to the three-dimensional honeycomb nature of geocell, it is capable of generating several mechanisms for improving the performance of foundations. A higher stiffness, bearing capacity and better pressure distributing characteristic could be achieved by incorporating single and multiple layers of geocell or planar reinforcement. Using such methods, the performance of a foundation bed is also much improved under cyclic loading of machines or vehicles. In this chapter, the advantages of geocell reinforcement compared to planar geotextile reinforcement are described under static

and repeated loading conditions. Then the usage of geocell and planar geotextile reinforcements are extended to multiple layers of geocell reinforcement. The results presented in this chapter are fully obtained from scaled models or full-scale experiments and thus, could provide a solid understanding for designing and construction of geocell-reinforced foundations.

4.6.1 Performance of Single Geocell Reinforcement Compared to Multiple Geotextile Reinforcement

Comprehensive results from laboratory model tests on strip footings with width of 75 mm supported on the geocell- and geotextile-reinforced sand beds with the same characteristics of geotextile are reported by Moghaddas Tafreshi and Dawson (2010a). The soil used is relatively uniform silica sand with grain sizes between 0.85 and 2.18 mm and with a specific gravity (G_s) of 2.68. It has a Coefficient of uniformity (C_u) of 1.35, Coefficient of curvature (C_c) of 0.95, an effective grain size (D_{10}) of 1.2 mm and mean grain size (D_{50}) of 1.53, which means that almost all the grains are between 1 and 2 mm in size. The maximum and minimum void ratios (e_{max} and e_{min}) of the sand were 0.82 and 0.54, respectively. According to the Unified Soil Classification System, the sand is classified as poorly graded sand with letter symbol SP (see Fig. 4.25a). The angle of internal friction of sand obtained through drained triaxial compression tests on dry sand samples at a relative density of 72% was 37.5 (all tests being run on dry sand at this relative density).


$D_{10} = 1.20$ mm
$D_{30} = 1.36$ mm
$D_{50} = 1.53$ mm
$D_{60} = 1.62$ mm
$C_u = 1.35$
$C_c = 0.95$

(a)   (b)
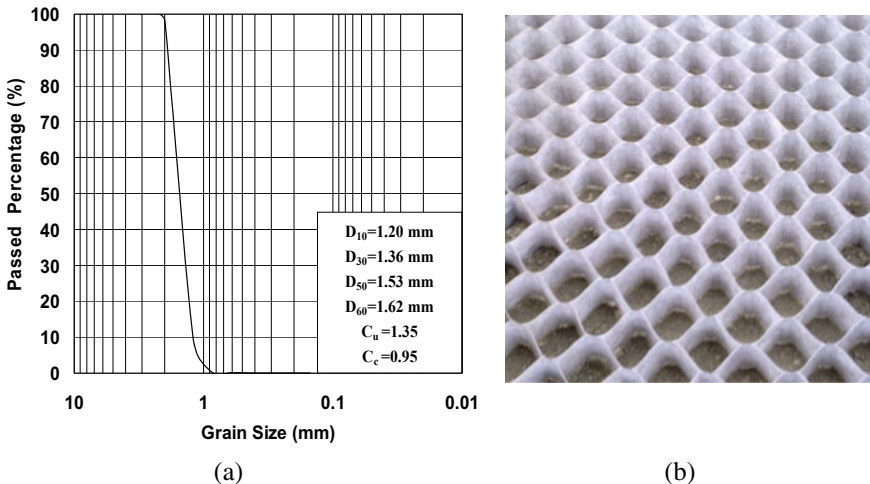
Fig. 4.25 **a** Particle size distribution curve **b** Isometric view of the geocell (Moghaddas Tafreshi and Dawson 2010a)

The geocell and geotextile layers used were both made and supplied by the same company. The geocell was fabricated from the same geotextile material that forms the planar geotextile. Geocells consist of a cellular structure manufactured from flexible, semi-flexible, or strong geosynthetics such as geotextile (see Fig. 4.25b). It comprises a polymeric, honeycomb-like structure with open top and bottom manufactured from strips of geotextile that are thermo-welded into a cellular system. The type of geotextile is nonwoven. The area weight (g/m^2), tensile strength (kN/m) and thickness under 200 kN/m^2 (mm) are 190, 13.1 and 0.47, respectively. When filled with soil or other mineral material, it provides an ideal surface for construction projects such as foundations, slopes, driveways, etc. The high tensile strength of both the weld and geotextile provide an ideal structure with high capacity that prevents infill from spreading thus hindering settlement. The pocket size (d) of the geocell used was kept constant (at $d = 50$ mm). It was used at heights (H) of 25, 50, and 100 mm in the testing program. The geocell and geotextile properties are the same throughout this chapter.

In order to provide a meaningful comparative assessment between the geotextile and geocell reinforcement, the quantity of material used must be matched. The quantity of material used in each test relative to that used in the least reinforced test is termed as 'a', which is equivalent to the mass of a single sheet of geotextile reinforcement of the smallest width used in the tests. Assessment of performance was undertaken for arrangements with geotextile sheet and geocell reinforcement of the same mass of geotextile being paired together. For example, the experiment reinforced by two layers of short geotextile reinforcement has exactly the same mass of geotextile as that reinforced by the short geocell reinforcement at $H/B = 0.66$ (see Fig. 4.26 for the definition of H and B). This pair both have two units 'a' of reinforcement the same as the long pair of one layer for geotextile or $H/B = 0.33$ for geocell reinforcement. It should be noted that the amount of material used in each test is a function of reinforcement width and of the number of layers of geotextile or height of geocell reinforcement.

Geocell benefits are assessed in terms of increased bearing capacity of a strip footing subjected to a monotonically increasing load. Provision of the geocell reinforcement in reinforcing the sand layer significantly increases the load-carrying
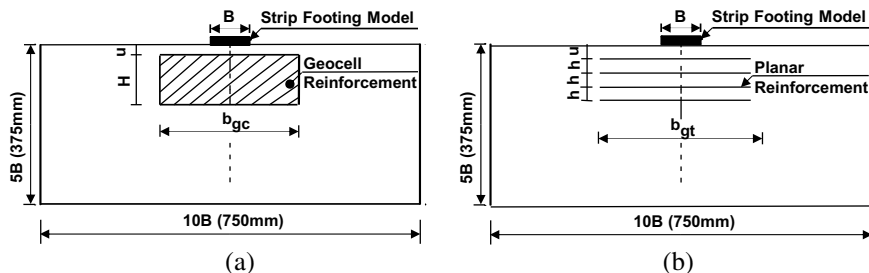
Fig. 4.26 Geometry of the **a** geocell-reinforced foundation bed **b** geotextile-reinforced foundation bed (Moghaddas Tafreshi and Dawson 2010a)

capacity, reduces the footing settlement, and decreases the surface heave of the footing bed more than the geotextile reinforcement with the same characteristics and the same mass used. Overall, with an increase in the number of geotextile reinforcement layers, the height of geocell reinforcement, and the reinforcement width, the bearing pressure of the foundation bed increases and the footing settlement decreases. Thus, the efficiency of reinforcement decreases by increasing the above parameters. A detailed discussion on the effect of different parameters (as shown in Fig. 4.26) will be presented hereafter.

An important factor for obtaining the best performance in soil reinforcement is the embedment depth (u) and width of reinforced layer (b_{gc} for geocell and b_{gt} for geotextile layer- see Fig. 4.26). The optimum depth of the topmost layer of geocell reinforcement is approximately 0.35 times the footing width ($u/B = 0.35$), while the depth to the top of the geocell should be approximately 0.1 times of the footing width ($u/B = 0.1$). The vertical spacing of the geotextile layers was selected to be equal to u/B and held constant in all the tests at $h/B = 0.35$. The tests performed with different reinforcement widths (short, medium and long reinforcement width) indicate that increasing the reinforcement width more than 4.2 and 5.5 (i.e., long width) times the footing width for the geocell and geotextile reinforcement, respectively, would not provide much additional improvement in bearing pressure.

Figure 4.27 shows the bearing pressure with footing settlement (s/B) for the geocell-reinforced, planar-reinforced, and unreinforced beds. From this figure, it may be clearly observed that with increasing the mass of reinforcement (increase in the height of the geocell reinforcement; *H/B* or in the number of layers of geotextile reinforcement; *N*); both stiffness and bearing pressure (bearing pressure at a specified settlement) considerably increase. In the case of the unreinforced sand bed, it is apparent that the bearing capacity failure has taken place at a settlement equal to 12% of footing width while in case of both the geocell- and geotextile-reinforced

Fig. 4.27 Variation of bearing pressure with settlement for the geocell and geotextile reinforcement with Long width ($b_{gc}/B =$ 4.2 and $b_{gt}/B = 5.5$, see Fig. 4.26 for the definition of b_{gc} and b_{gt}), (Moghaddas Tafreshi and Dawson 2010a)
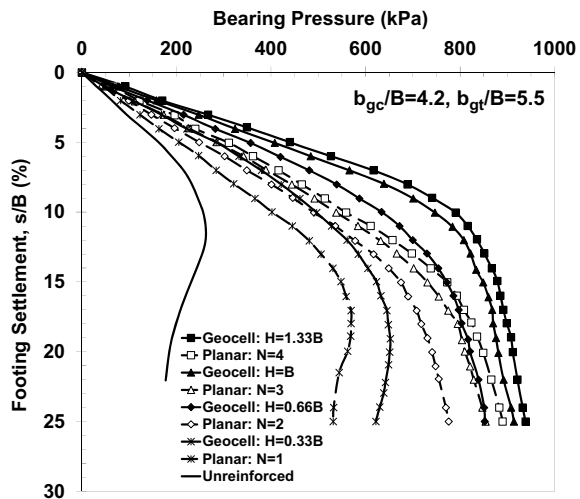
sand beds; no clear failure point is evident for the larger masses of reinforcement ($N \geq 2$ or $H/B \geq 0.66$). Beyond a settlement of 10–16% there is a reduction in the slope of the pressure-settlement curve. However, when lightly reinforced ($N = 1$ and $H/B = 0.33$, respectively, for geotextile reinforcement and geocell reinforcement) failure is observed at settlements of 16–18% with clear post-failure reductions in bearing capacity.

The performance improvement due to the provision of reinforcement is represented using non-dimensional improvement factor of IF which compares the bearing pressure of the geotextile or geocell reinforcement bed to that of the unreinforced bed at a given settlement, s_i.

$$\text{IF}_{\text{gt}} = \frac{q_{\text{geotextile}}}{q_{\text{unrein.}}} \text{ OR IF}_{\text{gc}} = \frac{q_{\text{geocell}}}{q_{\text{unrein.}}} \quad s_i / B = 2, 4, 6, 8, 10 \text{ and } 12\% \qquad (4.53)$$

where q_{unrein}, $q_{\text{geotextile,}}$ and q_{geocell} are, respectively, the values of bearing pressure of the unreinforced bed, the geotextile-reinforced bed, and the geocell-reinforced bed.

The variation of these two parameters, IF_{gt} and IF_{gc} with footing settlement for long, medium, and short reinforcement width are shown in Fig. 4.28. According to this figure, it is evident that for the same mass of geotextile material used in the tests at the settlement level of 4%, the maximum improvement in bearing capacity (IF) was obtained as 2.73 and 1.88 with the provision of geocell and the equivalent geotextile reinforcement, respectively. Therefore, improvement of foundation performance is proved and it can be concluded that geocell provides more benefits compared to geotextile forms of reinforcement. For amounts of settlement that are tolerated in practical applications, improvements in bearing capacity greater than 200% can be achieved with the application of geocell reinforcement, whereas geotextile reinforcement arrangements can only deliver 150% for these two quantities, respectively.

In many applications, the foundation is subjected to a number of load repetitions and hence, it is also essential to figure out the reinforced foundation performance under repeated loading. Moghaddas Tafreshi and Dawson (2010b) performed a series of laboratory model tests on strip footings supported on geocell and geotextile-reinforced sand beds under a combination of static and repeated loads. Footing settlement due to initial static applied load and up to 20,000 subsequent load repetitions was recorded until its value becomes stable or failure occurred due to excessive settlement. The typical scheme of repeated loading with the definition of static and dynamic loads is presented in Fig. 4.29. The properties of the material used in these tests are similar to the static tests describe previously (see the beginning of Sect. 4.1).
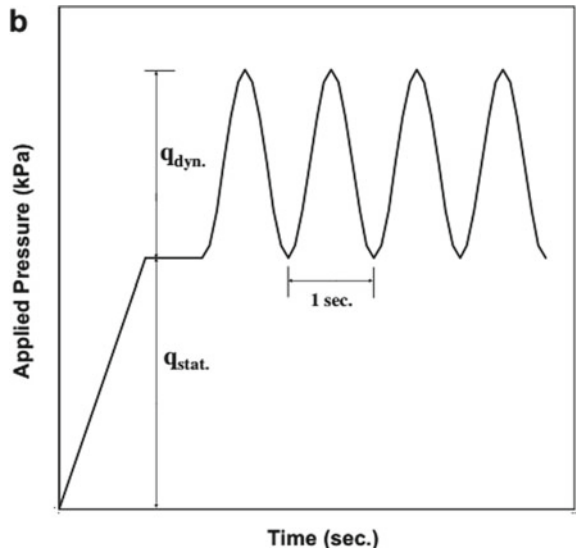
The variation of the footing settlement, s/B, at the peak of each load pulse with the number of load cycles as a consequence of the repeated loading pattern (as illustrated in Fig. 4.29), is plotted in Fig. 4.30 for unreinforced, geotextile-reinforced, and geocell-reinforced sand beds. The reinforced cases had the same mass of geotextile ($N = 2$ and $H/B = 0.66$). Based on Fig. 4.30, using the geocell reinforcement, or the planar geotextile reinforcement with the number of layers greater than 1, leads
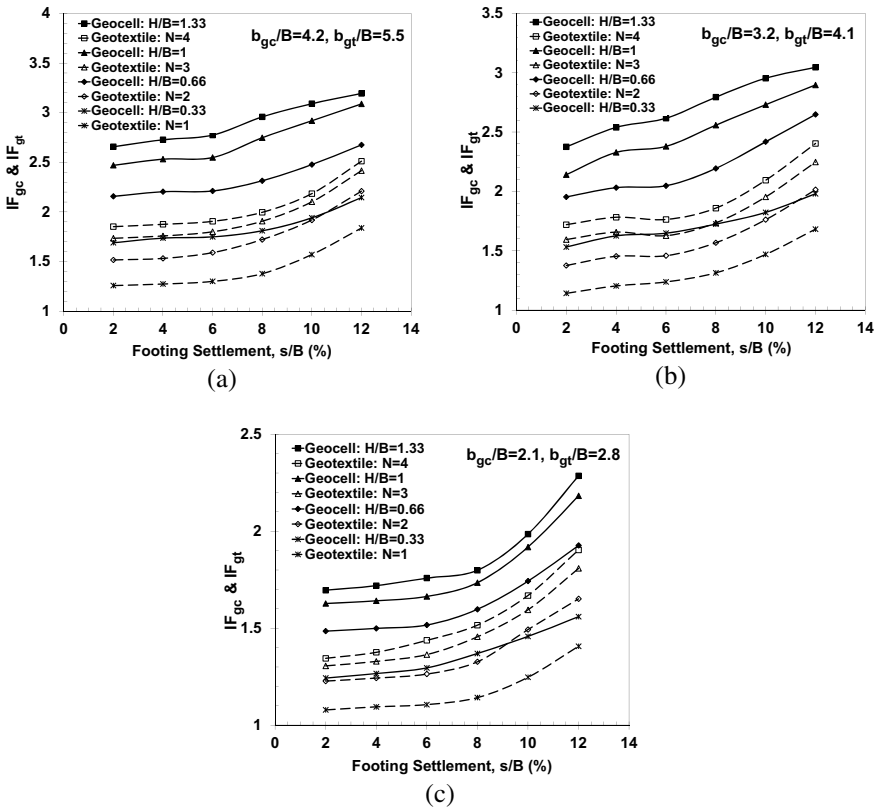
Fig. 4.28 Variation of the bearing capacity improvement factor (IF) with footing settlement for the geocell and geotextile reinforcement, **a** Long width ($b_g/B = 4.2$ and $b_p/B = 5.5$), **b** medium width ($b_g/B = 3.2$ and $b_p/B = 4.1$) and **c** short width ($b_g/B = 2.1$ and $b_p/B = 2.8$), (Moghaddas Tafreshi and Dawson 2010a)

to stabilizing behavior, irrespective of the repeated load level, q_{dyn}/q_{stat}, whereas no-reinforcement ($q_{dyn}/q_{stat} = 30$ and 50%) or under reinforcement ($N = 1$ for geotextile at $q_{dyn}/q_{stat} = 50\%$) allows excessive settlement and unstable behavior to develop. The only unreinforced bed to show a stabilizing response was that loaded at $q_{dyn}/q_{stat} = 20\%$ which became stable at a maximum (shakedown) settlement, s/B, equal to 9.11% at approximately 15,400 load cycles. In the case of the unreinforced sand beds under repeated loading, it is apparent that the excessive settlement commenced at about 3700 cycles (e.g., point X on Fig. 4.30) and 170 cycles, respectively, for repeated load amplitudes that were 30 and 50% of static load (q_{dyn}/q_{stat}). For the experiment containing one layer of geotextile reinforcement ($N = 1$) and subjected to a repeated loading amplitude that was 50% of the static load ($q_{dyn}/q_{stat} = 50\%$), the excessive settlement commenced at about 2220 cycles. This point of inflexion in the number of cycles versus the settlement curve appears to evidence a change in the internal behavior of the sand. After this number of cycles, unstable behavior

Fig. 4.29 Typical time
history of initial static and
repeated load on footing
(Moghaddas Tafreshi and
Dawson 2010b)

Fig. 4.30 Variation of the
footing settlement (s/B) with
number of applied load
repetitions for the
unreinforced, geocell (H/B
$= 0.66$), and geotextile ($N =$
2) reinforced beds. Loading
amplitude of repeated loads
(q_{dyn}/q_{stat}) was 20, 30 and
50%, (Moghaddas Tafreshi
and Dawson 2010b)
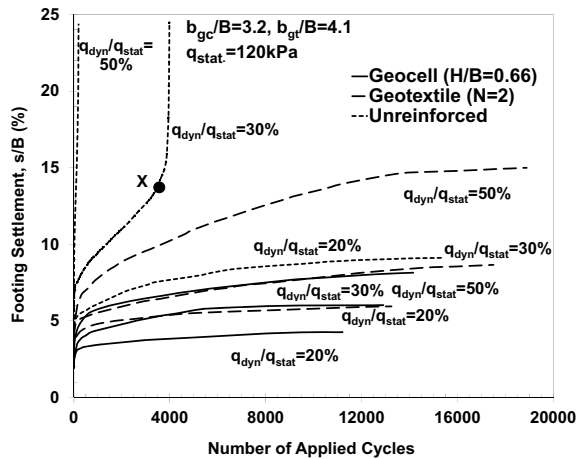
develops and the value of s/B accelerates with further load applications. When a non-stabilizing response is observed, due to excessive footing settlement, a significant heave of the fill surface starts. This response indicates that the unreinforced soil, or soil-reinforcement composite material with a small mass of reinforcement, when subjected to strong repeated loads, ruptures locally in the region under and around the footing, permitting large settlements. In the case of the geocell reinforcement and the geotextile reinforcement (with $N > 1$), an initial, rapid settlement during the first load applications is followed by a secondary settlement at a slower rate. Finally, the settlement rate of the footing is very small or insignificant.

Fig. 4.31 Variation of the maximum footing settlement (*s/B*) with amplitude of repeated loads for unreinforced and both the geocell and the geotextile-reinforced bed (Moghaddas Tafreshi and Dawson 2010b)
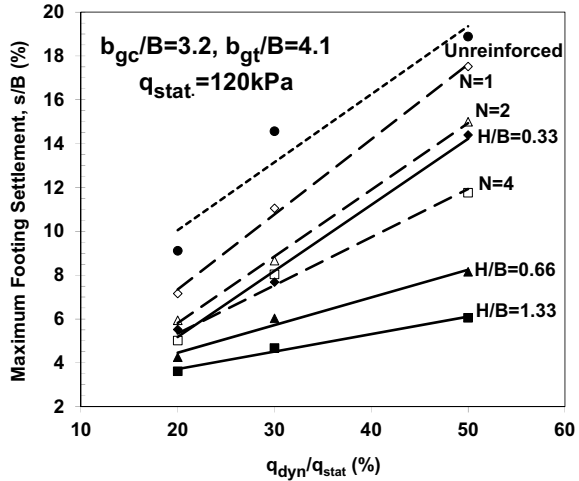

Figure 4.31 shows the variation of the maximum footing settlement (*s/B*) with an amplitude of repeated loads for the geocell-reinforced, geotextile-reinforced, and unreinforced beds. From this figure, it can be observed that, although there is some scatter, the footing settlement varies linearly with q_{dyn}/q_{stat}, irrespective of reinforcement type (geocell or geotextile) and amount. With an increase in the height of the geocell reinforcement or in the number of geotextile reinforcement layers the rigidity of the reinforced system increases or, to state this another way, the maximum value of footing settlement (*s/B*) decreases at any given q_{dyn}/q_{stat}. This implies that increasing the amount of reinforcement mass in the sand can control (lessen) the footing settlement and provide greater stability to a footing even under strong dynamic loads. Also, Fig. 4.31 makes plain that, even when comprising half the mass of geotextile material (*H/B* = 0.66 compared with *N* = 4), the geocell-reinforced sand can deliver a greater improvement (decrease) in the maximum settlement of the footing compared with the geotextile-reinforced one at any given q_{dyn}/q_{stat}.

Figure 4.32 summarizes the variation in the maximum footing settlement (non-dimensionalized as *s/B*) with number of applied load repetitions for the three geotextile-reinforced cases (*N* = 1, 2, 4) for the experiments with the three different heights of geocell reinforcement (*H/B* = 0.33, 0.66, 1.33) and for the unreinforced sand bed. The figure shows the results for the repeated loading case having an amplitude of 20% of applied static load (q_{dyn}/q_{stat} = 20%). The lines show the cumulative plastic and resilient settlement measured at the peak of each load pulse. It can be noted that the variation rate of peak footing settlement reduces as the number of cycles increase, and finally becomes stable after a certain number cycles, irrespective of the height of the geocell reinforcement (*H/B*) or the number of layers of geotextile reinforcement (*N*). This indicates that, where the total loading is insufficient to cause rupture within the soil system, reorientation of particles in the soil adjacent to the geotextile ceases relative rapidly, the system becomes stable and can be said to have

Fig. 4.32 Variation of the footing settlement (*s/B*) with number of applied load repetitions at $q_{dyn}/q_{stat} = 20\%$ for the unreinforced, geocell-reinforced and geotextile-reinforced beds (Moghaddas Tafreshi and Dawson 2010b)
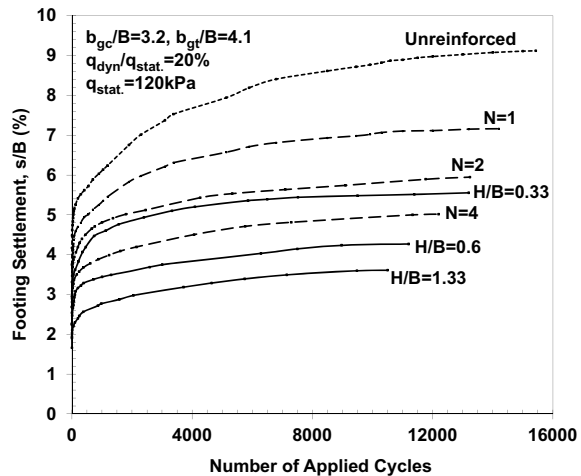

reached a state of plastic shakedown (Werkmeister et al. 2005). On the other hand, the magnitude of footing settlement increases with the number of cycles and reaches a sensibly constant maximum value at the number of load cycles. The maximum footing settlement, s/B, is considerably decreased relative to the unreinforced one as a consequence of either increase in the height of the geocell reinforcement (*H/B*) or in the number of layers of geotextile reinforcement (*N*).

The performance of the geocell is much improved over that of the geotextile for the same mass of geotextile material used. The performance of reinforcement in decreasing the settlement of a sand bed subjected to dynamic loads of various amplitudes [either by adding geocell of increasing height (*H/B*) or by adding layers of the geotextile (*N*)], is the subject of Fig. 4.33. The variation of the maximum value of footing settlement (in terms of *s/B*) as a function of the number of layers of geotextile (*N*) and the height of geocell (*H/B*) is shown for the three repeated load amplitudes ($q_{dyn}/q_{stat} = 20$, 30 and 50%).

To summarize, it can be concluded that, the rate of footing settlement decreases significantly as the number of loading cycles increases. Consequently, a resilient response condition, known as plastic shakedown, is achieved after 10,000–20,000 cycles dependent on the type and the mass of reinforcement and the magnitude of the repeated load applied to the footing. The largest portion of the footing settlement occurs after the first ten cycles. The ratio of footing settlement during the first ten to that achieved by the last cycle varies between 0.35 and 0.6. The magnitude of the maximum footing settlement and the number of cycles required to develop plastic shakedown of the footing are a function of the initial applied static load (q_{stat}), the amplitude of the repeated load (q_{dyn}) and the mass of reinforcement below the footing base (*N* and *H/B*). For a given value of amplitude of repeated load, with increase in the number of geotextile reinforcement layers and in the height of geocell reinforcement, the footing settlement decreases. The efficiency (expressed in relation to the mass of reinforcement) was decreased by increasing the above parameters. With an increase

Fig. 4.33 Variation of the maximum footing settlement (*s/B*) with number of layers of geotextile, or height of 3D, reinforcements under repeated loading of amplitude $q_{dyn}/q_{stat} = 20$, 30 and 50% (Moghaddas Tafreshi and Dawson 2010b)
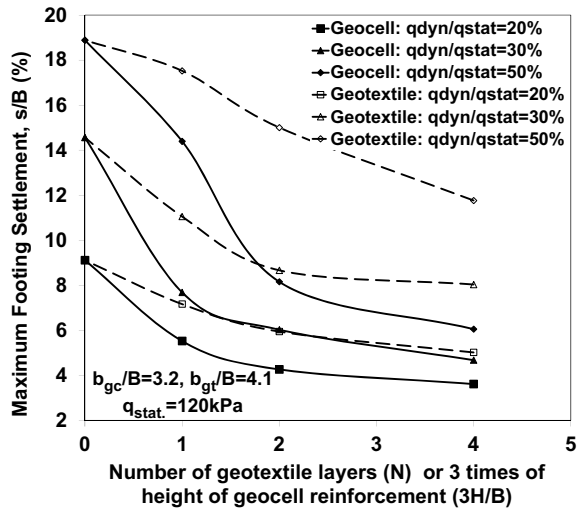

4.6.2 Performance of Multiple Geocell and Geotextile Reinforcement Layers

The previous section showed that geocell reinforcement can be significantly more effective than a geotextile, in improving the behavior of foundation beds under static and repeated loads. The evident benefit of using multiple geotextile or geogrid layers (e.g., Sitharam et al. 2005; Sitharam and Sireesh 2005) suggests that the use of multiple geocell layers could be beneficial. Geosynthetic inclusions will be most effective if used in the zone significantly stressed by the footing—which may be over a depth of 1 or 2 diameters beneath the footing—i.e., over a depth of approximately 0.6–2 m for typical strip/rectangular footing widths. Since the heights of commercially produced geocells are usually standard and most manufacturers of geocell produce them only at heights less than 200 mm, the use of a 0.6–2 m thick layer of geocell beneath the footing is impossible. Even if it were, such a thick geocell layer would likely make compaction of cell-fill extremely difficult, probably negating any reinforcement benefit. Hence, the use of several layers of geocell (say, three or four) each with a thickness ≤200 mm and with vertical spacing between successive layers of geocell is a practical alternative and could be a beneficial means of reinforcing the soil beneath a footing.

Moghaddas Tafreshi et al. (2016) performed a series of laboratory model tests on a model circular footing with 112.8 mm diameter (*D*), supported on multi-layered
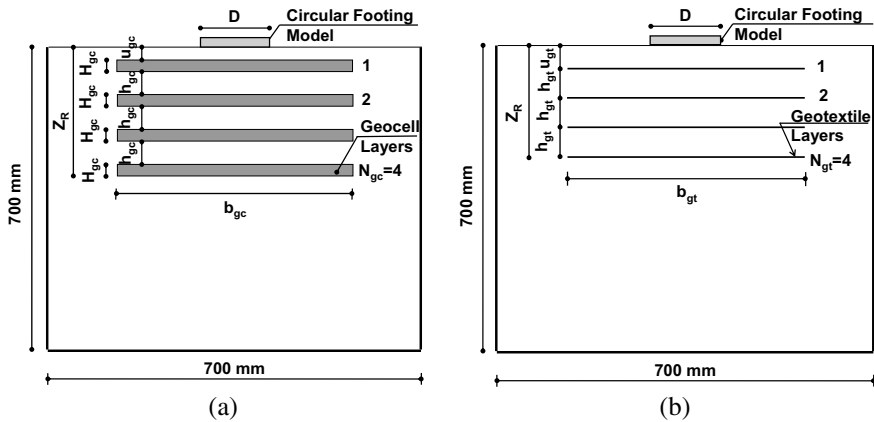
Fig. 4.34 a Layout of the multi-layered geocell-reinforced installation, **b** Layout of the multi-layered geotextile-reinforced installation (Moghaddas Tafreshi et al. 2016)
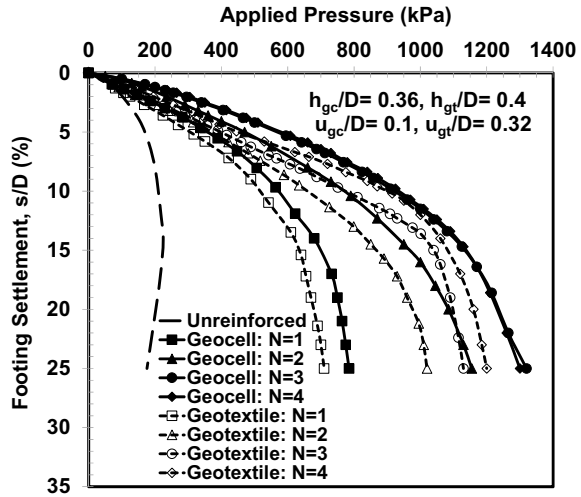
of geocell and geotextile-reinforced sand beds. Figure 4.34 shows the test setup and parameters used for the evaluation of such pavement systems, according to studies by Moghaddas Tafreshi et al. (2016).

The width of the geocell and geotextile layers (b_{gc} for geocell and b_{gt} for geotextile) and the depth to the top of the first geocell and geotextile layer below the footing (u_{gc} for geocell and u_{gt} for geotextile) are expressed in non-dimensional form with respect to footing diameter (D). In a previous study by Moghaddas Tafreshi and Dawson (2010a) optimum values of these parameters were $b_{gc}/D = 3.2$, $b_{gt}/D = 4.1$, $u_{gc}/D = 0.1$ and $u_{gt}/D = 0.32$. The same values were used and kept constant in the tests described here. The pocket size (d) of the geocell used was kept constant ($d = 50$ mm), while the geocell was used at a thickness (H_g) of 25 mm. The optimum vertical spacing of geocell reinforcement layers and geotextile reinforcement layers are approximately 0.36 and 0.4 times footing diameter ($h_{gc}/D = 0.36$ and $h_{gt}/D = 0.4$), respectively, which not reported here as detailed. The properties and classification of soil and geocell are identical to the previous section.

Figure 4.35 presents the bearing pressure-settlement behavior of geocell- and geotextile-reinforced foundations when the layers of geocell and geotextile were placed at ($u_{gc}/D = 0.1$ and $h_{gc}/D = 0.36$) and ($u_{gt}/D = 0.32$ and $h_{gt}/D = 0.4$), respectively. For any matching pair of geocell and geotextile reinforcement ($N_{gc} = N_{pt} = 1$; etc.), the width of geocell and geotextile reinforcement are kept constant (as before, at $b_{gc}/D = 3.2$, $b_{gt}/D = 4.1$, respectively) and the mass of geosynthetic material in the geocell will be 1.28 times less than that in its 'twinned' geotextile installation. It may be observed that as the layers of reinforcement are increased (increased mass of the geocell and geotextile reinforcement and consequent increase in the depth of the reinforced zone; Z_R), both the stiffness and bearing pressure (bearing pressure at a specified settlement) increase considerably. In the case of the unreinforced soil, it is apparent from Fig. 4.35 that the peak bearing pressure takes

Fig. 4.35 Variation of bearing pressure with settlement for the geocell and geotextile reinforcement ($h_{gc}/D = 0.36$, $h_{gt}/D = 0.4$), (Moghaddas Tafreshi et al. 2016)

place at a footing settlement equal to approximately 13% of footing diameter. In the case of both the geocell- and geotextile-reinforced soil, however, no clear failure point is evident.

The performance of the geocell reinforcement and geotextile reinforcement in increasing the subgrade modulus of a reinforced bed due to the increase in the number of the geocell layers (N_{gc}), or in the number of layers of the geotextile reinforcement (N_{gt}), is shown in Fig. 4.36. In this figure, a comparison can be drawn between an unreinforced bed, and the effect of the variation of the subgrade modulus improvement factor (Ik_{gc} and Ik_{gt}) with a number of reinforcement layers is indicated. The

Fig. 4.36 Variation of IF_{gc} and IF_{gt} with the number of geocell layers and geotextile layers (N_{gc} and N_{gt}) at different levels of settlement ($s/D = 4$, 8 and 12%) for $h_{gc}/D = 0.36$ and $h_{gt}/D = 0.4$ (Moghaddas Tafreshi et al. 2016)
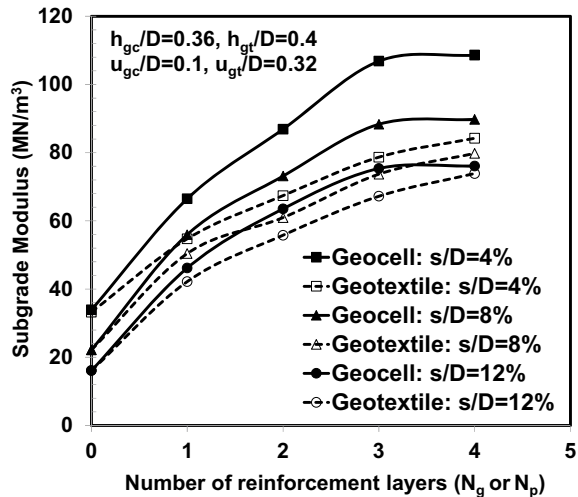
subgrade modulus improvement factor (Ik) at different footing settlements is defined as $Ik_p = k_p/k_{un}$ *for the geotextile reinforcement* and as $Ik_g = k_g/k_{un}$ for the geocell reinforcement (where $k_{un.}$, k_p, and k_g are the subgrade modulus values of the unreinforced bed, the geotextile-reinforced bed and the geocell-reinforced bed at a given settlement, respectively). The subgrade modulus k, is the secant modulus (i.e. the slope of the line joining the point on the stress-settlement curve, at a given settlement, to the origin) calculated at different footing settlements.

In all situations, the values of Ik_{gc} and Ik_{gt} are larger at greater footing settlement for both geotextile and geocell cases, with greater reinforcement as the footing penetrates further. This is attributable to the greater mobilization of tensile strain in the reinforcement layers and to the confinement provided between layers by the reinforcement. For the multi-layered geocell, no significant improvement in performance is achieved when more than three ($N_{gc} = 3$) geocell layers are used. Therefore, when three layers of geocell are located at $h_{gc}/D = 0.36$, the maximum zone of soil that can usefully be reinforced extends to a depth of approximately 1.48D ($Z_R = 1.48D$). In contrast, Fig. 4.36 shows that the performance improvement due to the provision of geotextile reinforcement may continue beyond four layers ($N_{gt} = 4$ with a reinforcement zone of $Z_R = 1.52D$). Figure 4.36 also shows that improvement in subgrade modulus is greater for geocell reinforcement than for geotextile reinforcement, irrespective of the settlement ratio of the footing. For example, for $N_{gc} = N_{gt} = 3$ and a settlement ratio of $s/D = 4\%$, the geocell installation improves the subgrade modulus by as much as 84% more than the geotextile installation.

For most practical purposes, performance of reinforced systems at low footing settlement ratios, s/D (say, less than 2%) is critical, hence footing performance (in terms of subgrade modulus improvement factor, Ik_{gc} and Ik_{gt}) at such low settlements is made the subject of Fig. 4.37. Again, comparing the "twinned" geocell and geotex-

Fig. 4.37 Variation of IF$_{gc}$ and IF$_{gt}$ with the number of geocell layers and geotextile layers (N_{gc} and N_{gt}) at different levels of settlement ($s/D = 4$, 8 and 12%) for $h_{gc}/D = 0.36$ and $h_{gt}/D = 0.4$ (Moghaddas Tafreshi et al. 2016)
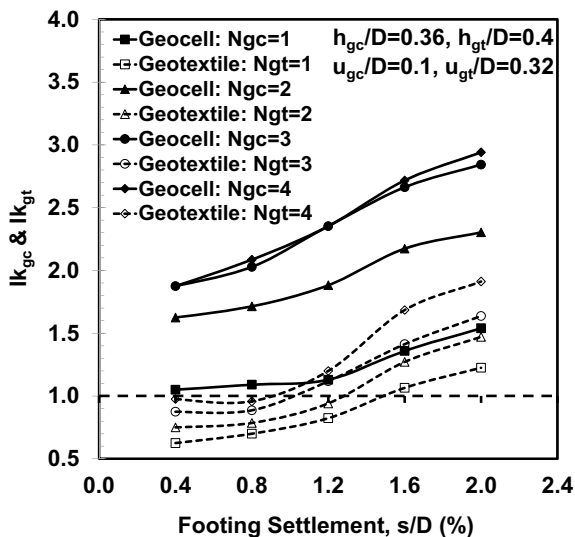
tile installations, the multi-layered geocell reinforcement system is both stiffer and more effective than the system with multi-layered geotextile reinforcement system. Furthermore, benefit of the geocell reinforcement is gained at very low settlement ratios ($s/D = 0.4\%$) whereas, in the case of geotextile reinforcement, the benefit only appears at footing settlement ratios of around 1–1.5%. At low settlements, apparently, before the geotextile has attracted loading to itself, geotextile installations may actually lead to a softer response than when unreinforced. The cause of this is uncertain but is probably indicative of lower geotextile-soil interface friction than soil–soil friction at a point in the loading sequence before the geotextile has been tensioned and is able to deliver benefit. Similar results were observed in the pressure-settlement of geotextile and geogrid reinforcement (Madhavi Latha and Somwanshi 2009) and of geocell reinforcement (Dash et al. 2001, 2003).

It is likely that the better performance at low settlement levels of the multi-layered geocell, compared with that of the multi-layered geotextile, is due to the geocell system gaining its resistance from the soil confinement that occurs when localized hoop stresses are developed in the walls of cells close (vertically and horizontally) to the footing. In a planar system, reinforcing action requires outward shear stress to be developed in the horizontal plane between the geotextile and soil throughout a zone whose size is controlled by the load spreading achieved in the soil between the footing and the uppermost geotextile layer. Such shear strains are not thought to be necessary for the geocell system, as localized compression alone will be sufficient to generate the hoop strain.

References

Aboobacker FMP, Saride S, Madhira MR (2015) Numerical modelling of strip footing on geocell-reinforced beds. Proc Inst Civ Eng Gr Improv 168(3):194–205

Abu-Farsakh M, Chen Q, Sharma R, Zhang X (2008) Large-scale model footing tests on geogrid-reinforced foundation and marginal embankment soils. Geotech Test J 31(5):413–423

American Society for Testing and Materials (ASTM) (2014) Standard test method for tensile properties of plastics. ASTM D638-14

Avesani Neto JO, Bueno BS, Futai MM (2013) A bearing capacity calculation method for soil reinforced with a geocell. Geosynthetics Int 20(3):129–142

Avesani Neto JO, Bueno BS, Futai MM (2015) Evaluation of a calculation method for embankments reinforced with geocells over soft soils using finite-element analysis. Geosynthetics Int 22(6):439–451

Biabani M, Indraratna B, Ngo NT (2016) Modelling of geocell-reinforced subballast subjected to cyclic loading. Geotext Geomembr 44(4):489–503

Binquet J, Lee KL (1975) Bearing capacity tests on reinforced earth slabs. J Geotech Eng ASCE 101(12):1241–1255

Brown SF, Kwan J, Thom NH (2007) Identifying the key parameters that influence geogrid reinforcement of railway ballast. Geotext Geomembr 25(6):326–335

BS8006 (1995) British standard: code of practice for strengthened/reinforced soils and other fills

Chen Q, Abu-Farsakh M, Sharma R, Zhang X (2007) Laboratory investigation of behavior of foundations on geosynthetic-reinforced clayey soil. Transp Res Rec: J Transp Res Board 2004:28–38

Cuelho E, Perkins S, Morris Z (2014) Relative operational performance of geosynthetic used as subgrade stabilization, Final Project Report, FHWA/MT-14-002/7712-251, Research Programs, State of Montana Department of Transportation, Montana, USA

Dash SK, Krishnaswamy NR, Rajagopal K (2001) Bearing capacity of strip footings supported on geocell-reinforced sand. Geotext Geomembr 19(4):235–256

Dash SK, Rajagopal K, Krishnaswamy NR (2007) Behavior of geocell reinforced sand beds under strip loading. Can Geotech J 44:905–916

Dash SK, Sireesh S, Sitharam TG (2003) Model studies on circular footing supported on geocell reinforced sand underlain by soft clay. Geotext Geomembr 21(4):197–219

Duncan JM, Chang CY (1970) Nonlinear analysis of stress and strain in soils. J Soil Mech Found Div 96(5):1629–1653

Foster CR, Ahlvin RG (1959) Stresses and deflections induced by a uniform circular load. Proc Highw Res Board 33:467–470

Góngora IAMG, Palmeira EM (2016) Assessing the influence of some soil-reinforcement interaction parameters on the performance of a low fill on compressible subgrade. Part II: Influence of surface maintenance. Int J Geosynthetics Gr Eng 2(1):18–29

Harikumar M, Sankar N, Chandrakaran S (2016) Behaviour of model footing resting on sand bed reinforced with multi-directional reinforcing elements. Geotext Geomembr 44(4):568–578

Harr ME (1966) Foundations of theoretical soil mechanics. McGraw-Hill, New York

Hegde AM, Sitharam TG (2015) Three-dimensional numerical analysis of geocell-reinforced soft clay beds by considering the actual geometry of geocell pockets. Can Geotech J 52(9):1396–1407

Hirai H (2008) Settlements and stresses of multi-layered grounds and improved grounds by equivalent elastic method. Int J Numer Anal Meth Geomech 32(5):523–557

Hirai H, Kamei T (2004) A method to calculate settlement, stress, failure and allowable stress of multi-layered ground by equivalent thickness theory. J Struct Constr Eng 581:79–86

Hirai H, Kamei TA (2003) A method to calculate settlement, stress and allowable stress of multi-layered ground. J Struct Constr Eng 573:81–88

Hsieh C, Mao HL (2005) A bench-scale performance test for evaluation of the geosynthetic reinforcement effects on granular base courses. In: ASCE, Geosynthetics research and development in progress, geo-frontiers, pp 1–11

Jenner CG, Basset RH, Bush DI (1988) The use of slip line fields to assess the improvement in bearing capacity of soft ground given by cellular foundation cushion installed at the base of an embankment. In: Proceedings of international geotechnical symposium on theory and practice of Earth reinforcement. Fukuoka, Japan, pp 209–214

Koerner RM (1998) Designing with geosynthetics. Prentice Hall, New Jersey

Kumar VV, Saride S (2016) Rutting behavior of geocell reinforced base layer overlying weak sand subgrades. Procedia Eng 143:1409–1416

Lambe TW, Whitman RV (1969) Soil mechanics. Wiley, New York

Latha GM, Murthy VS (2007) Effects of reinforcement from on the behavior of geosynthetic reinforced sand. Geotext Geomembr 25:23–32

Latha GM, Rajagopal K, Krishnaswamy NR (2006) Experimental and theoretical investigations on geocell-supported embankments. Int J Geomech 6(1):30–35

Li AL, Rowe RK (2008) Effects of viscous behaviour of geosynthetic reinforcement and foundation soils on embankment performance. Geotext Geomembr 26(4):317–334

Liu SY, Han J, Zhang DW, Hong ZS (2008) A combined DJM-PVD method for soft ground improvement. Geosynthetics Int 15(1):43–54

Liu Y, Deng A, Jaksa M (2019) Failure mechanisms of geocell walls and junctions. Geotext Geomembr 47(2):104–120

Madhavi Latha GM (2000) Investigation on the behavior of geocell supported embankments, Ph.D. thesis, Department of Civil Engineering, Indian Institute of Technology Madras, Chennai

Madhavi Latha GM, Dash SK, Rajagopal K (2009) Numerical simulation of the behavior of geocell reinforced. Int J Geomech ASCE 9(4):143–152

Madhavi Latha GM, Rajagopal K, Krishnaswamy NR (2006) Experimental and theoretical investigations on geocell-supported embankments. Int J Geomech ASCE 6(1):30–35

Madhavi Latha GM, Somwanshi A (2009) Bearing capacity of square footings on geosynthetic reinforced sand. Geotext Geomembr 27(4):281–294

McDowell GR, Harireche O, Konietzky H, Brown SF, Thom NH (2006) Discrete element modelling of geogrid-reinforced aggregates. Proc Inst Civ Eng—Geotech Eng 159(1):35–48

Meyerhof G, Hanna A (1978) Ultimate bearing capacity of foundations on layered soils under inclined load. Can Geotech J 15(4):565–572

Mhaiskar SY, Mandal JN (1996) Investigations on soft clay subgrade strengthening using geocells. Constr Build Mater 10(4):281–286

Moghaddas Tafreshi SN, Dawson AR (2010a) Comparison of bearing capacity of a strip footing on sand with geocell and with planar forms of geotextile reinforcement. Geotext Geomembr 28(1):72–84

Moghaddas Tafreshi SN, Dawson AR (2010b) Behaviour of footings on reinforced sand subjected to repeated loading–comparing use of 3D and planar geotextile. Geotext Geomembr 28(5):434–447

Moghaddas Tafreshi SN, Khalaj O, Dawson AR (2013) Pilot-scale load tests of a combined multilayered geocell and rubber-reinforced foundation. Geosynthetics Int 20(3):143–161

Moghaddas Tafreshi SN, Shaghaghi T, Tavakoli Mehrjardi Gh, Dawson AR, Ghadrdan M (2015) A simplified method for predicting the settlement of circular footings on multi-layered geocell-reinforced non-cohesive soils. Geotext Geomembr 43(4):332–344

Moghaddas Tafreshi SN, Sharifi P, Dawson AR (2016) Performance of circular footings on sand by use of multiple-geocell or-planar geotextile reinforcing layers. Soils Found 56(6):984–997

Noori B (2012) Experimental investigation of the behavior of geocell reinforced rubber soil mixture. M.Sc. thesis, Faculty of Civil Engineering, K.N. Toosi University of Technology, Tehran, Iran

Odemark N (1949) Investigations as to the elastic properties of soils and design of pavements according to the theory of elasticity, vol 77. Statens Vaginstitute, Meddelande, Stockholm, Sweden

Palmeira EM, Gongora IAMG (2016) Assessing the influence of soil reinforcement interaction parameters on the performance of a low fill on compressible subgrade. Part I: Fill performance and relevance of interaction parameters. Int J Geosynth Ground Eng 2(1):1–17

Palmer LA, Barber ES (1940) Soil displacement under a circular loaded area. Proc Highway Res Board 20:279–286

Pokharel SK (2010) Experimental Study on geocell-reinforced bases under static and dynamic loading. Ph.D. thesis. University of Kansas, USA

Presto (2008) Geoweb Load Support System—Technical Overview, Presto Products Company. Appleton, WI, USA

Rajagopal K, Krishnaswamy NR, Latha Madhavi (1999) Behavior of sand confined with single and multiple geocells. Geotext Geomembr 17(3):171–184

Rowe RK, Li AL (2005) Geosynthetic-reinforced embankments over soft foundations. Geosynthetics Int 12(1):50–85

Rowe RK, Taechakumthorn C (2008) Combined effect of PVDs and reinforcement on embankments over rate-sensitive soils. Geotext Geomembr 26(3):239–249

Sharma R, Chen Q, Abu-Farsakh M, Yoon S (2009) Analytical modeling of geogrid reinforced soil foundation. Geotext Geomembr 27(1):63–72

Sireesh S, Faby Mole PA, Madhav MR, Vijay Kumar R (2016) Non-linear response of geocell reinforced dense granular layer over weak soil under circular loading. Int J Geotech Eng 10(1):23–30

Sireesh S, Sitharam TG, Dash SK (2009) Bearing capacity of circular footing on geocellesand mattress overlying clay bed with void. Geotext Geomembr 27(2):89–98

Sitharam TG, Hegde A (2013) Design and construction of geocell foundation to support embankment on soft settled red mud. Geotext Geomembr 41:55–63

Sitharam TG, Sireesh S (2005) Behaviour of embedded footings supported on geocell reinforced foundation beds, geotech. Test J ASTM 28(5):452–463

Sitharam TG, Sireesh S, Dash SK (2005) Model studies of a circular footing supported on geocell-reinforced clay. Can Geotech J 42(2):693–703

Tavakoli Mehrjardi Gh, Behrad R, Moghaddas Tafreshi SN (2019) Scale effect on the behavior of geocell-reinforced soil. Geotext Geomembr 47(2):154–163

Tavakoli Mehrjardi Gh, Ghanbari A, Mehdizadeh H (2016) Experimental study on the behavior of geogrid-reinforced slopes with respect to aggregate size. Geotext Geomembr 44(6):862–871

Tavakoli Mehrjardi Gh, Khazaei M (2017) Scale effect on the behavior of geogrid-reinforced soil under repeated loads. Geotext Geomembr 45(6):603–615

Tavakoli Mehrjardi Gh, Moghaddas Tafreshi SN, Dawson AR (2012) Combined use of geocell reinforcement and rubberesoil mixtures to improve performance of buried pipes. Geotext Geomemb 34(October):116–130

Tavakoli Mehrjardi Gh, Moghaddas Tafreshi SN, Dawson AR (2013) Pipe response in a geocell reinforced trench and compaction considerations. Geosynthetics Int 20(2):105–118

Tavakoli Mehrjardi Gh, Moghadas Tafreshi SN, Dawson AR (2015) Numerical analysis on buried pipes protected by combination of geocell reinforcement and rubber-soil mixture. Int J Civ Eng 13(2B):90–104

Tavakoli Mehrjardi Gh, Motarjemi F (2018) Interfacial properties of geocell-reinforced granular soils. Geotext Geomembr 46(4):384–395

Terzaghi K (1943) Theoretical soil mechanics. Wiley, New York

Thakur JK, Han J, Pokharel SK, Parsons RL (2012) Performance of geocell-reinforced recycled asphalt pavement (RAP) bases over weak subgrade under cyclic plate loading. Geotext Geomembr 35(December):14–24

Vakili J (2008) A simplified method for evaluation of pavement layers moduli using surface deflection data. In: The 12th international conference of international association for computer methods and advances in geomechanics (IACMAG), Goa, India, 1–6

Wayne MH, Han J, Akins K (1998) The design of geosynthetic reinforced foundations. Paper presented at the Geosynthetics in foundation reinforcement and erosion control systems

Werkmeister S, Dawson AR, Wellner F (2005) Permanent deformation behavior of granular materials: the shakedown theory. Transp Res Board 6(1):31–57

Yang X, Han J, Pokharel SK, Manandhar C, Parsons RL, Leshchinsky D, Halahmi I (2012) Accelerated pavement testing of unpaved roads with geocell-reinforced sand bases. Geotext Geomembr 32(June):95–103

Yang Z (1974) Strength and deformation characteristics of reinforced sand. Ph.D. thesis, University of California, Los Angeles, CA, USA

Yin JH (2000) Comparative modeling study of reinforced beam on elastic foundation. J Geotech Geoenviron Eng 126(3):265–271

Yoon YW, Heo SB, Kim SK (2008) Geotechnical performance of waste tires for soil reinforcement from chamber tests. Geotext Geomembr 26(1):100–107

Zhang L, Qiangkang G, Guoping C (2010a) Effect of geo-cell reinforced soil structure used in flexible airfield pavement. In: ICLEM logistics for sustained economic development. ASCE, pp 1629–1635

Zhang L, Zhao M, Shi C, Zhao H (2010b) Bearing capacity of geocell reinforcement in embankment engineering. Geotext Geomembr 28:475–482

Zhao MH, Zhang L, Zou XJ, Zhao H (2009) Research progress in two direction composite foundation formed by geocell reinforced mattress and gravel piles. Chin J Highw Transp 22(1):1–10

Zhou HB, Wen XJ (2008) Model studies on geogrid- or geocell-reinforced sand mattress on soft soil. Geotext Geomembr 26:231–238